Spectrochimica Acta Part A: Molecular and Biomolecular Spectroscopy 311 (2024) 123969

Contents lists available at ScienceDirect

Spectrochimica Acta Part A:
Molecular and Biomolecular Spectroscopy

journal homepage: www.journals.elsevier.com/spectrochimica-acta-part-a-molecular-and-biomolecular-spectroscopy

Scaling-up VPT2: A feasible route to include anharmonic correction on large molecules

Marco Fusè [a], Giuseppe Mazzeo [a], Giovanna Longhi [a,b], Sergio Abbate [a,b], Qin Yang [c], Julien Bloino [d,*]

[a] Dipartimento di Medicina Molecolare e Traslazionale, Università di Brescia, Viale Europa 11, 25123, Brescia, Italy
[b] Istituto Nazionale di Ottica (INO), CNR, Research Unit of Brescia, c/o CSMT, VIA Branze 45, 25123, Brescia, Italy
[c] Institute of Organic Chemistry and Biochemistry, Czech Academy of Sciences, Flemingovo náměstí 542/2, 160 00, Prague, Czech Republic
[d] Scuola Normale Superiore, Piazza dei Cavalieri, 56125, Pisa, Italy

GRAPHICAL ABSTRACT

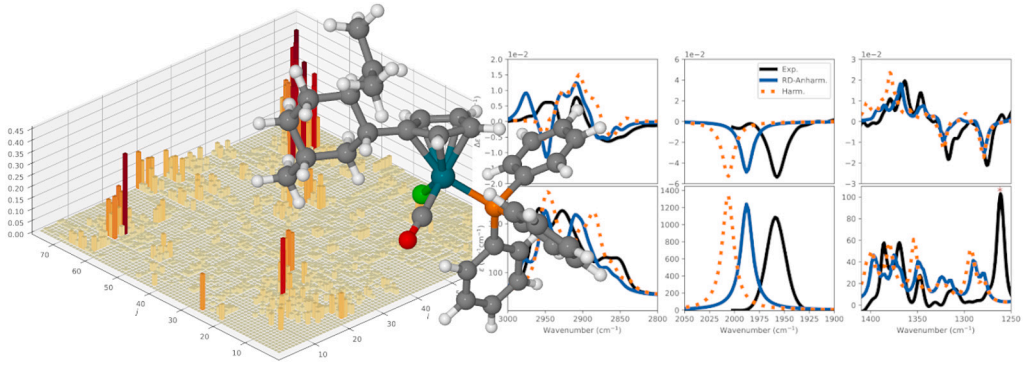

HIGHLIGHTS

- Anharmonic VPT2 simulations of large systems.
- Reduced-dimensionality scheme for anharmonic spectra of large systems with VTP2.
- Simple indicators to evaluate a priori the impact of truncated anharmonicity terms.
- New strategies to obtain converged spectra within selected spectral ranges.
- First anharmonic IR and VCD spectra of large ruthenium carbonyl complexes.

ARTICLE INFO

Keywords:
Vibrational circular dichroism (VCD)
Anharmonicity
Second-order vibrational perturbative theory (VPT2)
Reduced-dimensionality
Ruthenium complexes

ABSTRACT

Vibrational analysis plays a crucial role in the investigation of molecular systems. Though methodologies like second-order vibrational perturbation theory (VPT2) have paved the way to more accurate simulations, the computational cost remains a difficult barrier to overcome when the molecular size increases. Building upon recent advances in the identification of resonances, we propose an approach making anharmonic simulations possible for large-size systems, typically unreachable by standard means. This relies on the fact that, often, only portions of the whole spectra are of actual interest. Therefore, the anharmonic corrections can be included selectively on subsets of normal modes directly related to the regions of interest. Starting from the VPT2 equations, we evaluate rigorously and systematically the impact of the truncated anharmonic treatment onto

* Corresponding author.
E-mail addresses: marco.fuse@unibs.it (M. Fusè), julien.bloino@sns.it (J. Bloino).

https://doi.org/10.1016/j.saa.2024.123969
Received 2 October 2023; Received in revised form 18 January 2024; Accepted 24 January 2024
Available online 30 January 2024

simulations. The limit and feasibility of the reduced-dimensionality approach are detailed, starting on a smaller model system. The methodology is then challenged on the IR absorption and vibrational circular dichroism spectra of an organometallic complex in three different spectral ranges.

1. Introduction

Over the past decades, vibrational chiroptical spectroscopic techniques, principally vibrational circular dichroism (VCD) and Raman optical activity (ROA), have emerged as powerful and reliable tools to investigate molecular systems [1–4]. One strength of vibrational optical activity with respect to other chiroptical techniques is the possibility to be recorded for any chiral molecules without requiring any particular "active" groups.

With its almost fifty-year history, VCD is nowadays a consolidated technique, increasingly employed in industries, in particular for the characterization of drugs, where the enantiomeric definition is required by many drug agencies. Although its most successful application consists in assigning the absolute configuration, including complex cases where several sources of chirality are present [5–16], the wealth of information contained in the spectra can also be used to investigate the conformational flexibility or the interaction with the solvent for instance, and has inspired several applications [17–19]. Indeed, soon after its discovery, VCD has been successfully applied to the investigation of systems of biological relevance and biomolecules [20–23], including protein amyloid fibrils [24,25] and DNA [26,27]. VCD has also been recently applied to the investigation of catalytic reactions and liquid crystals [28–30].

With few exceptions [31,32], and contrary to their non-chiral counterparts, vibrational optical activity spectra can very rarely be interpreted by application of simple symmetry or empirical rules. Since the signal is the result of multiple interacting properties, the development of VOA spectroscopy and its adoption in laboratory workflows have gone conjointly with the development of theoretical models and their availability in computational software. Nowadays, for instance, VCD measurements can be directly paired with computations, using the harmonic-oscillator approximation coupled in most cases with density functional theory (DFT) [1,33].

However, as instruments and experimental techniques continue to evolve [34,35], they become able to produce spectra of higher resolution and access new energy ranges [36,37]. These new possibilities push standard approaches based on DFT and the harmonic oscillator to their limit, exposing their shortcomings [38].

One well-documented path to improvement is through a better description of the vibrational effects, with the inclusion of their intrinsic anharmonicity. Among available methods, vibrational perturbation theory (VPT), in particular its version at the second order [39], has attracted some attention, capable of accounting for the leading contributions of anharmonicity for a fraction of the cost of more sophisticated alternatives [40–46]. In brief, it builds upon the harmonic approximation through a perturbative inclusion of anharmonic effects. Different cutoffs in the expansion of the potential energy can be chosen. The order is defined with respect to the second-derivatives, which corresponds to the harmonic level, leading to VPT2 (up to the fourth derivative of the energy), VPT4 (sixth order), VPT6 (eighth order) and so on. Among them, VPT2 is a good compromise between accuracy and computational cost, requiring in practice only a limited expansion of the potential energy surface—and property surface for the intensities—which can be done through single numerical differentiations. Nonetheless, the additional cost over the harmonic approximation can become particularly high when targeting large systems, making even VPT2 inapplicable for these cases.

This is the case of many chiral metal complexes with important biological and technological roles, for instance in the enzymatic functions or in catalytic synthesis [48–52], which are often quite sizable. A few years ago, some of us have studied a complex of ruthenium(II) (RuCl, on the right side of Fig. 1), which can serve as a prototype to study the interaction of carbon monoxide with metal atoms [47]. From a spectroscopic perspective, an interesting feature is that the coordinated carbonyl ligand typically lies in the 2125–1850 cm^{-1} range, a region of the IR spectrum where only overtone and combination bands are usually observed [53,54]. The corresponding VCD signal revealed a clear correspondence with the configuration at the metal center, which can be used as a probe of the configuration of the metal center and that we confirm in this work experimentally in Fig. 2 with three closely related complexes obtained by halogen substitution (RuBr, RuI) or removal by silver tetrafluoroborate in acetronitrile solution ($RuBF_4$).

Unfortunately, at that time, the dimension of the complex did not consent performing simulations beyond the harmonic approximation, thus precluding a direct comparison between simulations and experiments and, for instance, the investigation of the CH-stretching region. Even now, the size remains a major hurdle for a full anharmonic treatment. This motivated us to study a feasible route to account for anharmonic effects on large molecules.

We may first note that, often, only portions of the whole spectra are investigated and/or are rich of useful VCD signals and therefore, as proposed before, anharmonic corrections can be narrowed to certain regions [55]. Because of the lack of analytic high-order derivatives for the energy and intensities in standard computational packages, anharmonic constants are constructed by sampling the potential energy and property surfaces. This means that, by design, it is possible to build them incrementally, so that they can be computed only on subsets of normal modes which are directly related to the regions of interest for a fraction of the computational cost required. However in this approach only a truncated anharmonic correction would be included, potentially leading to inaccurate results, especially for intensities, often more sensitive than the energy [36].

With the aim of reproducing the whole experimental band-shape in the region of interest, it is essential to understand how this truncation will impact the energies, but also the transition moments, the latter having been often overlooked in previous studies of this type. This has led us to investigate what a reduced-dimensionality VPT2 meant in terms of theory, accuracy, reliability. In this work, we focus on these aspects, and illustrate them first on a model system inspired by the full system, the template molecule depicted on the left side of Fig. 1, sufficiently large to be representative of potential issues in the real system, but small enough to still be feasible at the full VPT2 level. Then, the new protocol is applied to the full-size complex **RuCl**. The evident improvement in the simulated spectra with respect to the harmonic results paves the way to a better understanding of the vibrational pattern of this complex, but also offers an encouraging route to study more systematically large systems beyond the harmonic level.

The paper is organized as follows. After providing the theoretical background to VPT2 in the context of a reduced-dimensionality (RD) approach where only a subset of anharmonic constants are available, the experimental and computational details are given. Then, starting from the template molecule, we discuss the impact of the choice of the electronic structure method rooted in DFT, especially on vibrational optical activity spectra. Using the indicators provided in the theoretical part, we analyze the impact of the RD scheme on the simulation of energies and intensities of specific transitions. We then extend this work to spectroscopic ranges of the template molecule within the RD approach, and eventually scale up to the simulation of the IR absorption and VCD spectra in three spectral regions of the **RuCl** complex. We draw conclusions and outline perspectives for the RD approach in the last section.

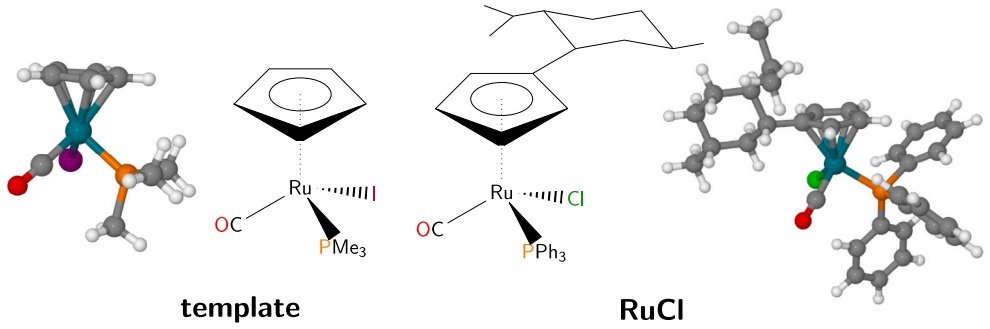

Fig. 1. Graphical representations of the investigated ruthenium complexes. On the left, the smaller template system is shown, while on the right the structure of the full molecular system **RuCl** is reported.

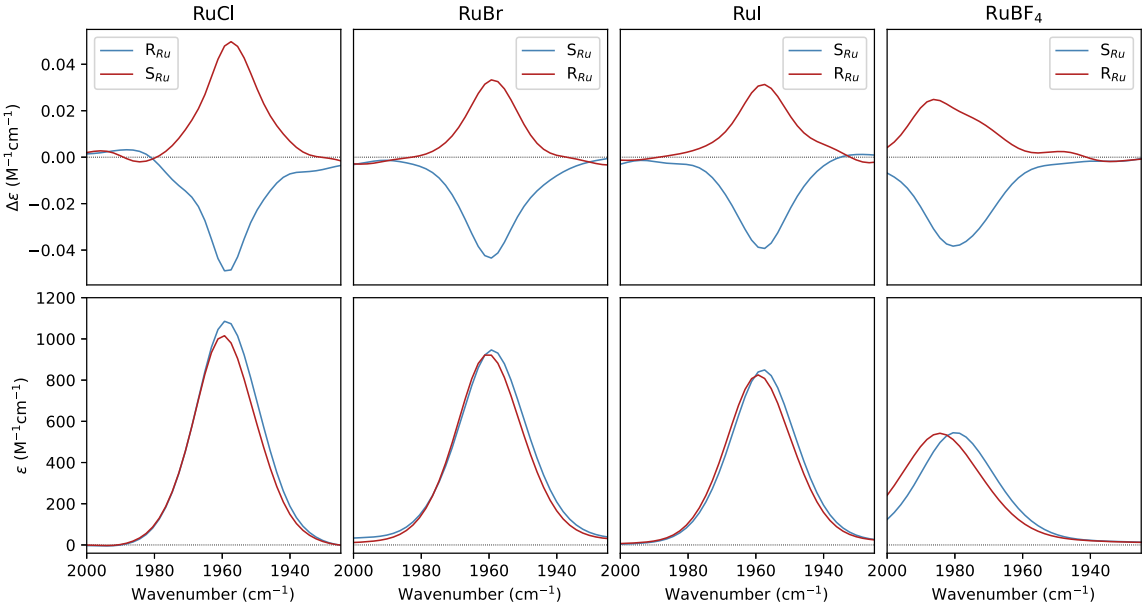

Fig. 2. Experimental IR and VCD spectra of **RuCl**, RuBr, RuI and $RuBF_4$ pairs of diastereomers (see Fig. **S1** in Supplementary Material) at the metal in the CO stretching region. **RuCl** data were taken from Ref. [47], other spectra were recorded in 0.08 M/CCl_4 solutions. An inversion in the correspondence between the signs and metal configurations of **RuCl** with respect to the others complexes reflects changes in the priority rules of the substituents. Thus, among the panels, the colors were kept consistent with the spatial arrangement.

2. Theoretical background

2.1. VPT2 energies

In absence of analytic forms, the third and fourth derivatives of the potential energy V required to compute the VPT2 energies are commonly obtained through the numerical differentiation of analytic second derivatives along the normal coordinates, either dimensionless ($\boldsymbol{q}$) or mass-weighted ($\boldsymbol{Q}$). Third derivatives (also called cubic force constants) can be built from single numerical differentiations, below shown with respect to $\boldsymbol{q}$ since the equations will be later given with respect to these quantities,

$$\mathrm{f}_{ijk} = \frac{\partial^3 V}{\partial q_i \partial q_j \partial q_k} = \frac{\mathrm{f}_{ij}(+\delta q_k) - \mathrm{f}_{ij}(-\delta q_k)}{2\delta q_k} = \frac{\mathrm{f}_{ik}(+\delta q_j) - \mathrm{f}_{ik}(-\delta q_j)}{2\delta q_j} = \frac{\mathrm{f}_{jk}(+\delta q_i) - \mathrm{f}_{jk}(-\delta q_i)}{2\delta q_i}, \quad (1)$$

While the construction of the fourth derivatives (quartic force constants) would require in theory a double differentiation, using two steps, a single step is needed in practice. Indeed, since only semi-diagonal quartic force constants are necessary for the VPT2 energies and most transition intensities (except for ternary '1+1+1' combinations, [56] see the Supplementary Material), the relevant quantities can be generated from the same displacement as the cubic ones,

$$\mathrm{f}_{iijk} = \frac{\partial^4 V}{\partial q_i \partial q_i \partial q_j \partial q_k} = \frac{\mathrm{f}_{jk}(+\delta q_i) + \mathrm{f}_{jk}(-\delta q_i) - 2\mathrm{f}_{jk}(\boldsymbol{q}^{\mathrm{eq}})}{{\delta q_i}^2} \quad (2)$$

$$\mathrm{f}_{iijj} = \frac{\mathrm{f}_{jj}(+\delta q_i) + \mathrm{f}_{jj}(-\delta q_i) - 2\mathrm{f}_{jj}(\boldsymbol{q}^{\mathrm{eq}})}{{\delta q_i}^2} = \frac{\mathrm{f}_{ii}(+\delta q_j) + \mathrm{f}_{ii}(-\delta q_j) - 2\mathrm{f}_{ii}(\boldsymbol{q}^{\mathrm{eq}})}{{\delta q_j}^2} \quad (3)$$

f_{ij} are the Cartesian force constants converted to the dimensionless coordinates, $\boldsymbol{q}^{\mathrm{eq}}$ refers to the equilibrium geometry and δq_i is an arbitrary step along normal coordinate q_i.

From these equations, some anharmonic force constants are defined multiple times. When the full necessary force field is built, by computing the harmonic force constants at $2N$ displaced geometries (N is

the number of normal modes), this redundancy can be used to check the stability of the numerical differentiation, since the constants should be equal. On the other hand, this means that the cost of building the anharmonic force field can be reduced by carrying out the numerical differentiation on a subset of P normal modes. The obvious drawback is that some non-redundant data may end up to be missing.

To evaluate the impact of the truncation on the anharmonic correction, let us consider the definition of the transition energy from the ground state to a vibrational state $|\psi_M^{\upsilon}\rangle$,

$$\nu_M = \varepsilon_M - \varepsilon_0 = \sum_{i=1}^{N} \upsilon_{M,i}\omega_i + \sum_{i=1}^{N}\sum_{j=i}^{N} \chi_{ij}\left[\upsilon_{M,i}\upsilon_{M,j} + \frac{1}{2}\left(\upsilon_{M,i} + \upsilon_{M,j}\right)\right] \quad (4)$$

where $\upsilon_{M,i}$ represents the number of quanta associated to mode i in state M, and ω_i its harmonic wavenumber. χ is the anharmonic correction matrix, whose elements are defined as,

$$16\chi_{ii} = \mathrm{f}_{iiii} - \frac{5\mathrm{f}_{iii}^{\,2}}{3\omega_i} - \sum_{\substack{j=1\\ j\neq i}}^{N} \frac{\left(8\omega_i^{\,2} - 3\omega_j^{\,2}\right)\mathrm{f}_{iij}^{\,2}}{\omega_j\left(4\omega_i^{\,2} - \omega_j^{\,2}\right)} \quad (5)$$

$$\begin{aligned} 4\chi_{ij} = {} & \mathrm{f}_{iijj} - \frac{2\omega_i\mathrm{f}_{iij}^{\,2}}{\left(4\omega_i^{\,2} - \omega_j^{\,2}\right)} - \frac{2\omega_j\mathrm{f}_{ijj}^{\,2}}{\left(4\omega_j^{\,2} - \omega_i^{\,2}\right)} - \frac{\mathrm{f}_{iii}\mathrm{f}_{ijj}}{\omega_i} - \frac{\mathrm{f}_{jjj}\mathrm{f}_{iij}}{\omega_j} \\ & + \sum_{\substack{k=1\\ k\neq i,j}}^{N}\left[\frac{2\omega_k\left(\omega_i^{\,2} + \omega_j^{\,2} - \omega_k^{\,2}\right)\mathrm{f}_{ijk}^{\,2}}{(\omega_i + \omega_j + \omega_k)(\omega_i - \omega_j - \omega_k)(\omega_j - \omega_i - \omega_k)(\omega_k - \omega_i - \omega_j)} - \frac{\mathrm{f}_{iik}\mathrm{f}_{jjk}}{\omega_k}\right] \\ & + \frac{4\left(\omega_i^{\,2} + \omega_j^{\,2}\right)}{\omega_i\omega_j} \sum_{\tau=x,y,z} B_{\tau}^{\mathrm{eq}}\{\zeta_{ij,\tau}\}^2 \end{aligned} \quad (6)$$

If we assume that the numerical differentiation has been carried out along a single normal mode i, to compute the anharmonic correction to the transition energy of the fundamental state $|1_i\rangle$ for instance, then the terms highlighted in orange in Eq. (6) are null since f_{jjj} and f_{jjk} are unknown. As already noted in Ref. [55], a common pattern can be noted for both terms, $\mathrm{f}_{jjj}\mathrm{f}_{iij}/4\omega_j$ and $\mathrm{f}_{iik}\mathrm{f}_{jjk}/4\omega_k$, which can be recast in the form, $\alpha_i(j)\mathrm{f}_{jjj}$ and $\alpha_i(k)\mathrm{f}_{jjk}$, with $\alpha_i(j)$ defined as,

$$\alpha_i(j) = \frac{\mathrm{f}_{iij}}{4\omega_j} \quad (7)$$

Since all terms of $\alpha_i(j)$ are known from the differentiation along normal mode i, $\alpha_i(j)$ can be used as an indicator of the importance of the missing term. If $\alpha_i(j)$ or $\alpha_i(k)$ are very small, then the related term is likely small and will contribute marginally to the total correction of the energy. Conversely, if it is large, then the corresponding term may not be insignificant. This is also consistent with the fact that a large value of $\alpha_i(j)$ means that the associated cubic force constant is also high, and so is the coupling between modes i and j. Hence, the latter mode should also be treated at the anharmonic level. It is thus possible to devise an incremental strategy by selecting first the modes of interest, for instance a probe vibration or all the modes associated to a group of transitions in a specific region, and build the anharmonic force constants along these modes. Then, by computing for each mode the corresponding function $\alpha_i(j)$, one can identify the larger couplings that can contribute to the VPT2 energies of the states of interest. If the couplings involve modes previously not selected, then additional numerical differentiations are carried out along these modes and their couplings evaluated. The procedure can be carried out iteratively until convergence, that is to say all substantially coupled modes are included in the anharmonic treatment and the correction to the energy of the states of interest stabilizes.

It is convenient at this point to introduce some terms to qualify the different types of modes in the anharmonic treatment. In the following, a mode is defined *active* if the differentiation was carried out along this mode and the anharmonic correction is included in the transition energies of its fundamental states and overtones. On the opposite, a mode will be labeled *inactive* if the anharmonic force constants are not specifically constructed along this normal mode. In practice, this means that the numerical differentiation is not carried out along this mode. Since the anharmonic correction would result significantly truncated, it is not applied to the transition energy of the fundamental and overtones of such a mode. By extension, the anharmonic correction will be applied to the energy of a combination band only if all the excited modes are active. For instance, the vibrational transition energy of the combination band $|1_i 1_j\rangle$ will be calculated at the VPT2 level only if both i and j are active. In addition to those two kinds, we introduce another type of mode, that will be called *passive* (or *frozen*) and is substantially a variant of *inactive*. Inactive modes still contribute indirectly to the anharmonic correction, which means that if i is active and j is inactive, any third derivatives of the energy involving both modes (f_{ijj}, f_{iij} and f_{ijk}) or any fourth derivatives of the form f_{iijk} (k can be equal or different from j and i) will be known and included in the anharmonic correction. On the other hand, if j is passive, then the contribution of any force constant involving this mode is neglected ($\mathrm{f}_{ijj} = \mathrm{f}_{iij} = \mathrm{f}_{ijk} = 0$, $\mathrm{f}_{iijk} = 0$ even if i is active). This can be convenient when dealing with large amplitude motions (LAMs), which are known to be poorly handled by VPT2. Indeed, LAMs can impact negatively the energies of other states through their couplings. Hence, a simple remedy can be to ignore any contribution from these modes, considering them passive. It should be kept in mind, however, that the coupling in this way is arbitrarily severed, so that such a technique should be applied with caution.

Turning back to the analysis of the coupling, since the primary use of the indicator α is its magnitude, it is more convenient to plot directly $\bar{\alpha}_i(j) = |\alpha_i(j)|$. It is worth mentioning that, contrary to the indicator used in a previous work [55], which only considered the cubic force constant, the quantity here is dimensionless, making the definition of a threshold in principle easier. Two strategies can be thus followed. Once all values of $\bar{\alpha}_i(j)$ for a given active mode i are computed, they are sorted by decreasing magnitude and the inactive modes j are added one-by-one in the anharmonic treatment until the anharmonic correction to the energies of the states of interest stabilizes. Considering the case of the fundamental of a probe vibration i, the transition energy has the form,

$$\nu_{1_i} = \omega_i + 2\chi_{ii} + \sum_{j\neq i}^{N} \frac{\chi_{ij}}{2} \quad (8)$$

The procedure described before translates in practice into "$\sum_{j\neq i} \frac{\chi_{ij}}{2}$" not changing anymore with the addition of new active modes j. It is noteworthy that if j is active, then f_{jjj} and f_{jjk} are available, so the corresponding term χ_{ij} is known exactly.

An alternative strategy, which does not require this progressive approach could be to set a threshold κ_E and consider active all the modes j for which $\bar{\alpha}_i(j)$ meets the condition,

$$\bar{\alpha}_i(j) \geq \kappa_E$$

This makes such protocol faster to implement and execute since there is no need for a systematic control every time a mode is added into the set of active modes. However, the difficulty is shifted to the choice of a suitable value of κ_E. This will be further investigated in the discussion on an actual case study.

2.2. VPT2 intensities

The indicator and strategies described in the previous section to build a reduced anharmonic force field are intrinsically connected to the calculation of VPT2 energies. The complete prediction of the vibrational band-shape requires also the accurate calculation of the intensities for at least the transitions of interest. This would typically mean that at the anharmonic level, in addition to the force field, the

expansion of the property surface is necessary. Like for the potential energy, analytic formulas are available for limited derivative orders, typically the first derivatives, and higher orders are obtained through numerical differentiations. It is important here, for reasons that will be clearer later, to separate properties depending on the nature of the first derivatives, with respect to either the nuclear coordinates or to their conjugate momenta.

Considering a generic property **P** function of $\boldsymbol{q}$, the necessary anharmonic terms to compute the intensities of fundamentals, first and second overtones, and 2-modes combinations up to 3 quanta ($|1_i 1_j\rangle$, $|2_i 1_j\rangle$) [57], can be obtained from the numerical differentiation of analytic first derivatives (noted as $\mathbf{P}_i$ for convenience),

$$\mathbf{P}_{ij} = \frac{\partial^2 \mathbf{P}}{\partial q_i \partial q_j} = \frac{\mathbf{P}_i(+\delta q_j) - \mathbf{P}_i(-\delta q_j)}{2\delta q_j} = \frac{\mathbf{P}_j(+\delta q_i) - \mathbf{P}_j(-\delta q_i)}{2\delta q_i} \tag{9}$$

$$\mathbf{P}_{iij} = \frac{\partial^3 \mathbf{P}}{\partial q_i \partial q_i \partial q_j} = \frac{\mathbf{P}_j(+\delta q_i) + \mathbf{P}_j(-\delta q_i) - 2\mathbf{P}_j(\boldsymbol{q}^{\mathrm{eq}})}{\delta {q_i}^2} \tag{10}$$

If **P** is function of the momenta, then there is no redundancy in the calculation of the second derivatives since $\mathbf{P}_{ij} \neq \mathbf{P}_{ji}$. Note that in the following, the order of the indexes is assumed to be this way, $\mathbf{P}_{ij} = \partial^2\mathbf{P}/\partial q_j \partial p_i$ and $\mathbf{P}_{ijk} = \partial^3\mathbf{P}/\partial q_k \partial q_j \partial p_i$.

The transition integral to a fundamental state $|1_i\rangle$ can be divided into two terms,

$$\langle \mathbf{P} \rangle_{0,1_i} = \langle \mathbf{P} \rangle^{i}_{0,1_i} + \langle \mathbf{P} \rangle^{\mathrm{off}}_{0,1_i} \tag{11}$$

where $\langle \mathbf{P} \rangle^{i}_{0,1_i}$ gathers the elements of $\langle \mathbf{P} \rangle_{0,1_i}$ that are known from the numerical differentiation with respect to q_i, and $\langle \mathbf{P} \rangle^{\mathrm{off}}_{0,1_i}$ all the other terms. Because of the subtle differences mentioned above between properties functions of $\boldsymbol{q}$ or of its conjugate momentum vector $\boldsymbol{p}$, the definition of both terms in the rhs of Eq. (11) will vary depending on **P**. It is nevertheless possible to obtain a general formulation by using a slightly different notation compared to Ref. [58]. The definition of the transition moment can be thus split into,

$$\begin{aligned}
\langle \mathbf{P} \rangle^{i}_{0,1_i} = {} & s_0 \times \mathrm{S} \times \mathbf{P}_i + \frac{s_2}{2}\mathbf{P}_{iii}(2+\mathrm{S}) - \frac{s_0}{8}\sum_{j=1}^{N} \mathrm{f}_{iijj}\mathbf{P}_j \left[\frac{1}{\omega_i + \omega_j} - \frac{\mathrm{S}(1-\delta_{ij})}{\omega_i - \omega_j}\right] \\
& - \frac{s_1}{4}\left\{\sum_{j=1}^{N} \mathrm{f}_{iij}\left(\frac{1+\delta_{ij}S}{2}\mathbf{P}_{ij} + \mathbf{P}_{ji}\right)\left[\frac{1}{3\omega_i} + \frac{\mathrm{S}}{\omega_j}\right]\right\} \\
& - \frac{s_1}{8}\left\{\sum_{j=1}^{N} \frac{\mathrm{f}_{ijj}}{\omega_i}\mathbf{P}_{ii}(1+3\mathrm{S}) + \sum_{j=1}^{N} \frac{\mathrm{f}_{iij}}{\omega_j}\left[2\mathrm{S}\mathbf{P}_{ji} + (1+\mathrm{S})\mathbf{P}_{ij}\right]\right\} \\
& + \frac{s_0}{2}\sum_{j,k=1}^{N}\left(\sum_{\tau} B^{\mathrm{eq}}_{\tau}\zeta_{ik,\tau}\zeta_{jk,\tau}\right)\mathbf{P}_j \left\{\frac{\sqrt{\omega_i\omega_j}}{\omega_k}\left(\frac{1}{\omega_i + \omega_j} + \frac{\mathrm{S}(1-\delta_{ij})}{\omega_i - \omega_j}\right)\right. \\
& \left. - \frac{\omega_k}{\sqrt{\omega_i\omega_j}}\left(\frac{1}{\omega_i + \omega_j} - \frac{\mathrm{S}(1-\delta_{ij})}{\omega_i - \omega_j}\right)\right\} \\
& + \frac{s_0}{16}\sum_{k,l=1}^{N} \mathrm{f}_{ikl}\mathrm{f}_{ikl}\mathbf{P}_i \left\{(1+\delta_{ik})(1-\delta_{il})\left[\frac{1}{2\omega_i(\omega_i + \omega_k + \omega_l)} - \frac{1}{2\omega_i(\omega_i - \omega_k - \omega_l)}\right.\right. \\
& \left.\left. + \frac{\mathrm{S}}{2(\omega_i + \omega_k + \omega_l)^2} - \frac{\mathrm{S}}{2(\omega_i - \omega_k - \omega_l)^2}\right]\right\} \\
& + \frac{s_0}{16}\sum_{j,k=1}^{N} \mathrm{f}_{iik}\mathrm{f}_{ijk}\mathbf{P}_j \left\{(1-\delta_{ij})(1-\delta_{ik})\left[\frac{4}{\omega_k(\omega_i + \omega_j)} + \frac{2}{(\omega_i + \omega_j)(2\omega_i + \omega_k)}\right.\right. \\
& \left. - \frac{4\mathrm{S}}{\omega_k(\omega_i - \omega_j)} - \frac{2\mathrm{S}}{(\omega_i - \omega_j)(2\omega_i + \omega_k)}\right] + \frac{\delta_{ij}}{\omega_i\omega_k}\left(1 + \frac{\delta_{ik}(6-4\mathrm{S})}{9}\right) \\
& \left. + \frac{5}{3}\delta_{ik}(1-\delta_{ij})\left[\frac{2}{\omega_i(\omega_i + \omega_j)} - \frac{2\mathrm{S}}{\omega_i(\omega_i - \omega_j)}\right]\right\} \\
& + \frac{s_0}{16}\sum_{j,l=1}^{N} \mathrm{f}_{iij}\mathrm{f}_{ill}\mathbf{P}_j \left\{\frac{\delta_{ij}}{\omega_i\omega_k}\left(1 + \frac{\delta_{il}(6-4\mathrm{S})}{9}\right)\right. \\
& \left. + (1-\delta_{ij})(1 + \frac{2\delta_{il}}{3})\left[\frac{2}{\omega_i(\omega_i + \omega_j)} - \frac{2\mathrm{S}}{\omega_i(\omega_i - \omega_j)}\right]\right\}
\end{aligned} \tag{12}$$

$$\begin{aligned}
\langle \mathbf{P} \rangle^{\mathrm{off}}_{0,1_i} = {} & \frac{s_2}{2}\sum_{\substack{k=1 \\ k\neq i}}^{N}\left\{\mathbf{P}_{kik} + \mathbf{P}_{ikk} + \mathrm{S}\mathbf{P}_{kki}\right\} - \frac{s_1}{8}\sum_{\substack{k=1 \\ k\neq i}}^{N}(1-\mathrm{S})\mathbf{P}_{ik}\mathrm{f}_{iik}\left[\frac{1}{3\omega_i} + \frac{\mathrm{S}}{\omega_k}\right] \\
& - \frac{s_1}{8}\sum_{\substack{j,k=1 \\ j,k\neq i}}^{N}\left\{\mathrm{f}_{ijk}\left(\mathbf{P}_{jk} + \mathbf{P}_{kj}\right)\left[\frac{1}{\omega_i + \omega_j + \omega_k} - \frac{\mathrm{S}}{\omega_i - \omega_j - \omega_k}\right]\right. \\
& \left. + \frac{\mathrm{f}_{jjk}}{\omega_k}\left[2\mathrm{S}\mathbf{P}_{ki} + (1+\mathrm{S})\mathbf{P}_{ik}\right]\right\} \\
& - \frac{s_0}{8}\sum_{j=1}^{N}\sum_{\substack{k=1 \\ k\neq i}}^{N}\mathrm{f}_{ijkk}\mathbf{P}_j\left[\frac{1}{\omega_i + \omega_j} - \frac{\mathrm{S}(1-\delta_{ij})}{\omega_i - \omega_j}\right] \\
& + \frac{s_0}{16}\sum_{\substack{j,k,l=1 \\ j,k,l\neq i}}^{N}\mathrm{f}_{ikl}\mathrm{f}_{jkl}\mathbf{P}_j\left\{\frac{1}{(\omega_i + \omega_j)(\omega_i + \omega_k + \omega_l)}\right. \\
& - \frac{1}{(\omega_i + \omega_j)(\omega_i - \omega_k - \omega_l)} \\
& \left. - \frac{\mathrm{S}}{(\omega_i - \omega_j)(\omega_i + \omega_k + \omega_l)} + \frac{\mathrm{S}}{(\omega_i - \omega_j)(\omega_i - \omega_k - \omega_l)}\right\} \\
& + \frac{s_0}{16}\sum_{\substack{k,l=1 \\ k,l\neq i}}^{N}\mathrm{f}_{iik}\mathrm{f}_{llk}\mathbf{P}_i\left[\frac{1}{\omega_i\omega_k}\right] \\
& + \frac{s_0}{16}\sum_{\substack{j,k,l=1 \\ j,k,l\neq i}}^{N}\mathrm{f}_{ijk}\mathrm{f}_{llk}\mathbf{P}_j\left[\frac{2}{\omega_k(\omega_i + \omega_j)} - \frac{2\mathrm{S}}{\omega_k(\omega_i - \omega_j)}\right]
\end{aligned} \tag{13}$$

where S, s_0, s_1, s_2 are constants whose values depend on the actual property and are reported in Ref. [58] for the spectroscopic techniques of interest here. The summations indexes were chosen so that each element would be fully known if mode k is active, with the only exception of $\mathbf{P}_{jk}$ in the case of non-commutating indexes (first derivatives of the properties with respect to the momenta). Compared to the energy, the definition of the intensities of fundamentals involve more complex couplings between several modes. No simple strategy can be established to assess *a priori* the extent of the couplings as done before. The problem is further complicated by the presence of different types of contributions, pure electrical (first term in the rhs of Eq. (13)), mixed electrical–mechanical (second and third terms), and pure mechanical, where electrical refers to the expansion of the property beyond the harmonic level, and mechanical to that of the vibrational wavefunction, hence the potential energy surface. Because of their different natures, a meaningful discussion is only possible by separating these three kinds of contributions.

The pure electrical anharmonicity requires numerical differentiations along all normal modes—$\mathbf{P}_{kik}$ and $\mathrm{S}\mathbf{P}_{kki}$ cancel each other for **P** function of the momenta [58] since S = −1—it is thus impossible to predict *a priori* the overall contribution of those terms. A possible indicator, albeit indirect, could be to evaluate the relative magnitude of the diagonal term with respect to the harmonic term,

$$\alpha^{E}_{i}(i) = \frac{\frac{s_2}{2}\mathbf{P}_{iii}(2+\mathrm{S})}{s_0 \times \mathrm{S} \times \mathbf{P}_i} \rightarrow \bar{\alpha}^{E}_{i}(i) = \left|\frac{s_2\mathbf{P}_{iii}(2+\mathrm{S})}{2s_0\mathbf{P}_i}\right|$$

Very low contributions could hint at a modest effect of the pure electrical anharmonicity as a whole, minimizing the need to explicitly extend the anharmonic property surface.

The problem of the mixed terms (second and third terms in the rhs of Eq. (13)) is more challenging in a way since it involves two distinct modes in addition to i and both mechanical (cubic force constants) and electrical (second derivatives of the properties) anharmonicities. The first term is specific to the case where the first derivative of **P** is with respect to the momenta. The known part, $2s_1\mathrm{f}_{iik}(1/3\omega_i - 1/\omega_k)/8$ is similar in form to $\alpha_i(k)$. Considering that $1/3\omega_i - 1/\omega_k \geq 1/\omega_k$ only

if $\omega_k \geq 6\omega_i$, and the wavenumbers of the modes typically of interest would be at least in the fingerprint region ($\omega_i \geq 600$ cm^{-1}), then $\bar{\alpha}_i(k)$ can act as an upper bound to estimate the magnitude of the term. The other term is common to any definition of **P** and can be subdivided into two components. In the first one, the cubic force constant is known. The largest contribution would come from

$$\frac{s_1}{8}\sum_{\substack{j,k=1\\ j,k\neq i}}^{N} \mathrm{f}_{ijk}\left(\mathbf{P}_{jk}+\mathbf{P}_{kj}\right)\frac{\mathrm{S}}{\omega_i-\omega_j-\omega_k}$$

which corresponds to a Fermi resonance for the intensity [36]. Since there is no way to distinguish between j and k, both would have to be taken into account. A mitigation strategy, to avoid including an excessively large number of active modes, would be to only consider critical cases, which would correspond to actual resonances. The latter will be discussed in more details later. Finally, for the last contribution to the mixed anharmonic term, only the property derivatives are in principle known (1 + S = 0 for the case where the indexes i and k cannot be interchanged). Since computing the anharmonic constants along mode k is sufficient to get the contribution of this term for any value of j, $|s_1\mathbf{P}_{ki}/4|$ could be used as an indicator. Since it is a purely electrical term, an indicator similar to $\alpha_i^E(i)$ can be employed,

$$\alpha_i^M(k)=\frac{\frac{\mathrm{S}s_1}{4}\mathbf{P}_{ki}}{s_0\times\mathrm{S}\times\mathbf{P}_i}\rightarrow\bar{\alpha}_i^M(k)=\left|\frac{s_1\mathbf{P}_{ki}}{4s_0\mathbf{P}_i}\right|$$

Finally, identifying the importance of the missing terms in the pure mechanical anharmonicity represents the most challenging task for several reasons. First, multiple modes are involved through the summations, which complicates the identification of a suitable indicator. Second, the largest contributions are expected to be the terms with a difference "$\omega_i - \omega_j$" at the denominator, which would correspond to 1-1 Darling–Dennison resonances (DDRs). Like what was proposed for the Fermi resonances above, protocols to identify 1-1 DDRs could be applied to identify potentially strong couplings [36,58–60]. However, this strategy has several limitations. The most obvious one is that it can only help identify couplings between i and a single mode, j. Another, subtler deficiency is that the terms used to identify such resonances, be it the actual Darling–Dennison term [61] or wave function coefficients [36,60] for instance, are themselves truncated. For instance, the total equation for the second-order coefficient of the VPT2 wave function is [36],

$$\begin{aligned}C^{(2)}_{1_i,1_j}=&\frac{1}{\omega_i-\omega_j}\left\{\sum_{k,l=1}^{N}\left\{\frac{1}{32}\mathrm{f}_{ikk}\mathrm{f}_{jll}\left[-\frac{1}{\omega_j}+\frac{1}{\omega_i}\right]\right.\right.\\&+\frac{1}{16}\mathrm{f}_{ikl}\mathrm{f}_{jkl}\left[-\frac{1}{\omega_j+\omega_k+\omega_l}+\frac{1}{\omega_i-\omega_k-\omega_l}\right]\\&\left.+\frac{1}{16}\mathrm{f}_{ijl}\mathrm{f}_{kkl}\left[-\frac{1}{\omega_l}+\frac{1}{\omega_i-\omega_j-\omega_k}\right]\right\}\\&\left.+\sum_{k=1}^{N}\frac{1}{8}\mathrm{f}_{ijkk}+\sum_{\tau}B_{\tau}^{\mathrm{eq}}\sum_{k=1}^{N}\zeta_{ik}\zeta_{jk}\left[\frac{\omega_k}{\sqrt{\omega_i\omega_j}}+\frac{\sqrt{\omega_i\omega_j}}{\omega_k}\right]\right\}\end{aligned}\tag{14}$$

Similar equations are found for the Darling–Dennison terms (Eqs. 118–121 in Ref. [61]). Only the Coriolis term (last term in Eq. (14)) is fully known if j, k and l are inactive, so that the only contributions from the anharmonic force field would be for the cases where $k = i$ ($\mathrm{f}_{ikl}\mathrm{f}_{jkl}$, $\mathrm{f}_{ijl}\mathrm{f}_{kkl}$, f_{ijkk}) or $l = i$ ($\mathrm{f}_{ikk}\mathrm{f}_{jll}$, $\mathrm{f}_{ikl}\mathrm{f}_{jkl}$, $\mathrm{f}_{ijl}\mathrm{f}_{kkl}$). While the incomplete summations can be sufficient to hint at a possible resonance between $|1_i\rangle$ and $|1_j\rangle$ and thus at a non-negligible coupling between the corresponding modes, it cannot act as a complete indicator to find all relevant contributions to the mechanical anharmonicity. Hence, the latter needs to be carefully monitored, by first focusing on the convergence of the energy while building up the list of active modes.

Moving beyond fundamentals, states can be divided between overtones and combinations. For a '1+1' binary combination, the transition moment can be written as,

$$\begin{aligned}\langle\mathbf{P}\rangle_{0,(1+\delta_{ij})_i(1-\delta_{ij})_j}=&\sqrt{\frac{2}{1+\delta_{ij}}}\times\left[\frac{s_1\times S}{2}\left(\mathbf{P}_{ij}+\mathbf{P}_{ji}\right)\right.\\&\left.+\frac{s_0}{4}\sum_{k=1}^{N}\mathrm{f}_{ijk}\mathbf{P}_k\left(\frac{\mathrm{S}}{\omega_i+\omega_j-\omega_k}-\frac{1}{\omega_i+\omega_j+\omega_k}\right)\right]\end{aligned}\tag{15}$$

All terms are thus known with i and j active. Obviously, the transition moment of the first overtone (case $j = i$ in the previous equation) is also fully known with i active.

For completeness, a formula for three-quanta transitions is given in the Supplementary Material (Eq. (1)), considering the most general case where i, j and k can be different ('1+1+1' ternary combination), and applicable to second overtones and '2+1' binary combinations. It is noteworthy that single numerical differentiations are insufficient to compute the full VPT2 correction to the intensity of ternary combinations, since the full quartic force field is necessary. The pure electrical contribution would be missing for the same reason. Actually, the latter problem arises also for '2+1' combinations with the transition moments of properties functions of the momenta since the indexes do not fully commute. Besides these limitations, considering that i, j and k are active, all terms are known for the cases where $\mathbf{P}_{mn} = \mathbf{P}_{nm}$. Otherwise, part of the mixed mechanical–electrical contributions would be missing.

2.3. Resonances

Resonances are a critical aspect of VPT2, and need to be properly treated to obtain reliable results. While strategies have been proposed in the literature to identify resonances through fixed criteria that could be implemented in black-box procedures [36,59,60,62–65], they have been devised considering full-dimensionality force fields. Their application to cases where only a subset of normal modes are "active" requires some clarification. For this purpose, it is convenient to separate the standard protocols to compute corrected VPT2 energies and intensities in two distinct steps, (i) the identification and removal of the resonant terms and (ii) their correction by mean of a variational method. Adopting our standard naming conventions, the first one will be labeled IDVPT2 (an extension of the original deperturbed VPT2 (DVPT2), which focused on the energies [63], to include the removal of Darling–Dennison resonances in the formulas of the transition moments for the intensities), while the full procedure including the second step corresponds to the generalized VPT2 (GVPT2). For simplicity, GVPT2 will be used to refer specifically to the variational part of the whole procedure.

After this brief presentation of the context, let us first focus on IDVPT2. Since resonances directly impact the quality of VPT2 results, they must be properly identified and removed. The protocol proposed in Ref. [36] has been adopted in this work. First, select states which are close in energy to be potentially in resonances. Second, estimate their probability of being actual resonances. This second step contains two complementary tests: one on the impact on the energy and one on the intensity. For Fermi resonances, the criterion proposed by Martin and coworkers [62] is used for the energy, and the magnitude of the first-order coefficient of the VPT2 wave function for the intensity. Darling–Dennison resonances do not impact directly VPT2 energies but some of them (1-1 DDRs for fundamentals and 1-3 DDRs for 3-quanta transitions) can affect the transition moments. The intensity-centric term relies on the second-order coefficient of the VPT2 wave function, reported in Eq. (14).

All terms potentially affected by Fermi resonances in the energy (Eqs. (5) and (6)) are known with i active, so that the tests can be carried out as usual. For the intensity, the only term primarily impacted

by Fermi resonances is related to the mixed electrical–mechanical contribution (Eq. (13)). Here again, all relevant elements are known so that the intensity-specific test can be carried out even if j and k are inactive. The other Fermi resonances in Eqs. (12) and (13) are embedded into the second-order wave function coefficient (Eq. (14)) and thus primarily related to the 1-1 Darling–Dennison resonance. As already detailed, this term is only partially known with a reduced anharmonic force field. Nevertheless, it remains an appropriate measure of a divergence in the VPT2 transition moments caused by a resonance condition. Hence, the tests on DDRs, like for Fermi resonances, are carried out over the whole ensemble of states, including active and inactive modes. It should be noted that, because all anharmonic force constants involving passive modes are canceled, any state including such modes cannot be in resonance.

The final GVPT2 energies are then obtained by computing the variational terms coupling each pair of states involved in resonances identified through the IDVPT2 scheme. Additional contributions can be included to account for the missing anharmonic effects in the VPT2 energies related to the Darling–Dennison couplings [66]. While tests on resonance are carried out over all inactive and active states, doing the same for the variational treatment could lead to an incorrect correction of the energy, since it should only be applied between states with IDVPT2/DVPT2 energies. As a consequence, the GVPT2 energies are only computed between "active" states. Hence, two strategies can be applied. If resonances are identified between active and inactive states, the modes involved in the latter can be set active and the anharmonic force field and property surfaces expanded. The energies and intensities are then corrected at the GVPT2 level. Otherwise, the variational correction is only partially applied.

3. Experimental and computational details

3.1. Experimental details

VCD measurements were carried out with a Jasco FVS6000 instrument, which is a FTIR instrument with an added linear polarizer and a ZnSe photo-elastic modulator to achieve VCD measurements. In the mid-IR and CO stretching regions, a liquid N_2-cooled HgCdTe (MCT) detector was employed. The resolution was set to 4 cm^{-1} in the range 2100–850 cm^{-1} and to 8 cm^{-1} in the range 2100–1800 cm^{-1}. The VCD spectra have been recorded in a solution of CCl_4 (concentration 0.04 M and 0.08 M), using a BaF_2 200 μm pathlength cell. For the CH-stretching region, a liquid N_2-cooled InSb detector was used (resolution 8 cm^{-1}). The sample was diluted in a CCl_4 solution (concentration 0.015 M) and placed in a quartz infrasil 1 mm pathlength cuvette. In all ranges, 6000 scans were accumulated for each spectrum and the reported data are averages over the accumulated spectra.

3.2. Computational details

All calculations were done at the density functional theory (DFT) level, using the SNSD basis set on light atoms [67], a double-ζ basis set which offers a good compromise between size and accuracy. It is constructed with the 6-31G(d,p) at its core, by adding the diffuse functions from aug-cc-pVDZ and one very tight s function for each non-hydrogen atom. For heavy atoms, the LanL2DZ basis set with effective core potentials to replace core electrons was chosen [68].

To minimize the errors in the numerical differentiation, very tight convergence criteria were used during the optimization step. In practice, this means that the maximum residual forces and displacements had to be smaller than 5×10^{-6} Hartree/Bohr and 2×10^{-5} Å, respectively. Numerical differentiations were carried out using a fixed step along the mass-weighted normal coordinates ($\delta Q_i = \sqrt{\hbar/2\pi c\omega_i} \times \delta q_i = 0.01\sqrt{\text{amu}}$ Å).

To match the experimental conditions, solvent effects were simulated by means of the polarizable continuum model (PCM) in its integral equation formalism, [69] with the default parameters of Gaussian16 [70].

To identify automatically the resonances, the protocol detailed in Ref. [36] and summarized in the previous section was used, with the following parameters:

- Fermi resonances:
  - Energy difference below 200 cm^{-1}
  - Energy-centric test: 1 cm^{-1}
  - Intensity-centric test: $|C^{(1)}_{1_i,1_j1_k}| \geq 0.1$
- 1-1 Darling–Dennison resonances:
  - Energy difference below 100 cm^{-1}
  - Energy-centric test: 10 cm^{-1}
  - Intensity-centric test: $|C^{(2)}_{1_i,1_j}| \geq 0.3$
- 2-2 Darling–Dennison resonances:
  - Energy difference below 100 cm^{-1}
  - Energy-centric test: 10 cm^{-1}

For the smaller system where the full anharmonic force field and property surfaces could be generated from single numerical differentiations and were thus available, the reduced forms were generated as follows. The full data sets were taken and the program checked if each element could be known when considering only the chosen ensemble of active modes. The actual value of cubic force constants were kept only if at least one index corresponded to an active mode. For quartic force constants of the form f_{iijk} ($j \neq k$), the quantity was set to 0 if i was not active. For f_{iijj}, the value was maintained if i or j was active. The first derivatives of all properties of interest here, that is to say the electric and the magnetic dipoles, are known analytically for the electronic structure calculation methods chosen in this work. Available derivatives with a reduced-dimensional treatment will depend on the property. For the electric dipole moment, $\mathbf{P}_{ij}$ is known if i or j is active, and $\mathbf{P}_{iij}$ only if i is active. For the atomic axial tensor (magnetic dipole), $\mathbf{P}_{ij}$ will be non-null only if j is active.

All electronic structure calculations were carried out with the Gaussian16 suite of quantum chemical programs [70]. The latest version of our code, implemented in a development version of Gaussian, was used for the VPT2 part.

4. Results and discussion

To analyze the impact of using a reduced-dimensional treatment on the anharmonic correction, a reference for which all required anharmonic constants are available is necessary. Building the full force field and property surface of the ruthenium organometallic complex reported on the right side of Fig. 1 would require at least 445 times the time necessary to compute the harmonic IR and VCD spectra on the same type of machine. Even by distributing over multiple computing units, this would still be a daunting task. A smaller, prototypical system was chosen instead (left panel in Fig. 1), named template in the following. The latter molecule has 75 normal modes. As comparison, on a mid-range machine (2-processors Intel Xeon 8-core E5-2667v2@3.30 GHz), a single "harmonic" calculation takes 4 min, compared to 8 h for the full system at the level of theory described in the computational details.

In order to establish a sound basis for our study, we need to confirm first the reliability of the overall theoretical model, which includes the electronic structure calculation methods and VPT2 corrections.

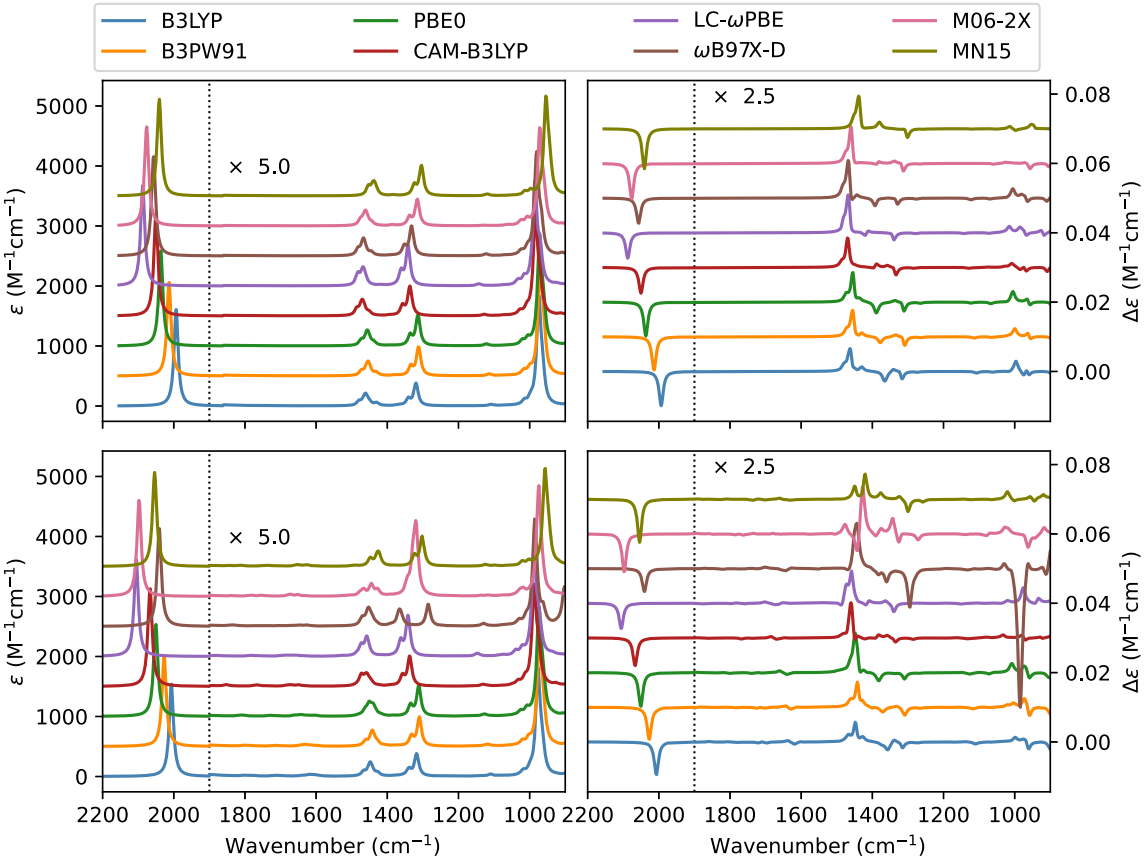

Fig. 3. Theoretical mid-IR absorption (left) and VCD (right) spectra of the template at the harmonic (top panels) and anharmonic (bottom panels) levels with different functionals. Lorentzian broadening functions with half-widths at half-maximum of 7 cm^{-1} were used to simulate the band shapes. A scaling factor of 0.98 was applied to the harmonic wavenumbers.

4.1. Full VPT2 treatment of the template molecule

As a perturbative approach, VPT2 depends intrinsically on the reference, here the harmonic approximation. On the other end, DFT functionals are well-known to give mixed performance depending on the system under study and the quantities of interest. With the large number of functionals available nowadays, finding a suitable candidate can be challenging. This is further complicated for anharmonic calculations by the fact that their behavior can be inconsistent beyond the harmonic level, which means that a functional can provide harmonic energies or intensities comparable to the best electronic structure methods but then predict poorly the anharmonic effects [64,71]. To illustrate this aspect, several popular exchange–correlation functionals have been selected, namely B3LYP [72,73], B3PW91 [72], PBE0 [74], CAM-B3LYP [75], LC-ωPBE [76], ωB97X-D [77], M06-2X [78] and MN15 [79].

The harmonic IR and VCD spectra are reported in the top panels of Figs. 3 and 4. Besides slight energy shift, the band-shape of the IR spectra in the mid-IR region (top left panel of Fig. 3) are quite similar. In the CH-stretching region (top left panel of Fig. 4), some more notable differences can be observed, especially for LC-ωPBE, which predicts the two main visible bands about 50 cm^{-1} higher in energies than the other functionals and with comparable heights, instead of having the lower-energy one about 50% more intense. More differences are observed between the tested functionals for the prediction of the VCD spectrum (top right panel of Fig. 4), with LC-ωPBE still diverging the most from the others. The pattern of peaks predicted around 3020–3000 cm^{-1} depending on the functionals are especially interesting elements of comparison. For B3PW91 and PBE0, a '+,–' pattern can be clearly seen, with the positive and negative bands of similar magnitudes. The positive band is significantly lower in intensity at the B3LYP, LC-ωPBE, ωB97X-D, M06-2X and MN15 levels. Finally, no positive band can be observed in that region with CAM-B3LYP, and only a negative band remains. The VCD spectrum in the mid-IR region (top right panel of Fig. 3) also presents variations between functionals, in particular for lower-intensity bands. The 1400–1300 cm^{-1} and 1100–900 cm^{-1} regions are interesting markers. Depending on the functionals, the former is dominated by either two negative bands (ωB97X-D, PBE0, B3PW91, B3LYP), a weak positive bulge and a negative band (MN15, CAM-B3LYP), or mostly a single negative band (LC-ωPBE, M06-2X). In the lower-energy region, the patterns are relatively similar between most functionals, except for M06-2X and MN15, which show significantly different structures, of lower intensity compared to the others.

This preliminary analysis already shows how the choice of the DFT exchange–correlation functional can affect the prediction of vibrational spectra. Because it primarily depends on the relative orientation of the transition moments of the electric and magnetic dipole, VCD is far more sensitive to minute changes in the geometry and electronic structure, making it an optimal test to validate the choice of the functionals.

Moving on beyond the harmonic-oscillator approximation, it is necessary to first check whether VPT2 is fully applicable on the target system. Indeed, the description of the anharmonic potential energy surface (PES) through a truncated polynomial expansion is not suitable for all vibrations. In some cases, a divergence in the terms of the expansion is observed, which then affect negatively the anharmonic correction. The perturbative treatment tends to amplify this effect, resulting in erroneous vibrational energies for the states involving such modes. To make matters worse, non-diagonal anharmonic force constants are often impacted, which leads to a chain contamination of the energies of other states through the mode couplings. It is thus

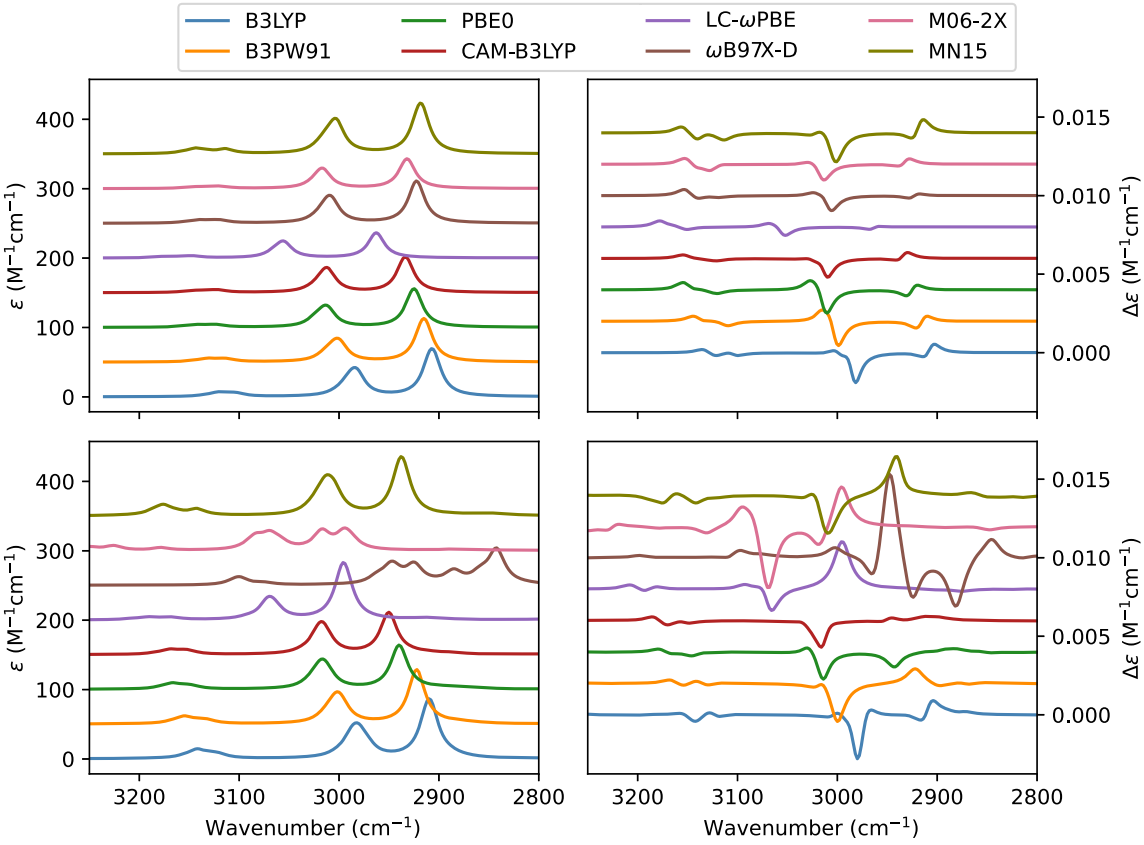

Fig. 4. Theoretical absorption (left) and VCD (right) spectra in the CH-stretching region of the template at the harmonic (top panels) and anharmonic (bottom panels) levels with different functionals. Lorentzian broadening functions with half-widths at half-maximum of 10 cm^{-1} were used to simulate the band shapes. A scaling factor of 0.95 was applied to the harmonic wavenumbers.

critical to identify precisely such a potential failure. The main difficulty is that there does not exist any univocal and formal definition of the modes that can be problematic, often collectively referred to as large amplitude motions (LAMs). Nevertheless, it is possible to identify them by checking some of their characteristics. Common types of LAMs are hindered rotational motions, and are identified visually or through the analysis of the internal coordinates describing the vibration [80]. This condition is, however, not sufficient, since the energy barrier for the rotation can be sufficiently high so that the local portion of the PES about the minimum is correctly described with a quartic expansion of the energy. As a matter of fact, another indicator of a possible LAM is a low harmonic frequency, typically below 150 cm^{-1}. The anharmonic force field can then help confirm the status of LAM for a given vibration. Excessively large third and fourth energy derivatives compared to the second derivatives (for instance, several times higher) are generally indicative of an over-correction. A final control are the VPT2 energies. Large corrections or, conversely, an increment compared to the harmonic values are signs of the potential presence of LAMs. For such a metric to be exploitable, all resonances must be correctly identified and removed to avoid false positives. This was done automatically using the protocol described in Ref. [36] with the parameters reported in the computational details. As a matter of fact, this family of systems represents an interesting problem for the detection of resonances. Indeed, as shown in Fig. **S2** in the Supplementary Material, standard tests used to identify Fermi resonances based purely on the energy failed to identify a resonance between the CO stretching fundamental and a combination because of the weak coupling. However, if not carefully handled, it causes a redistribution of the intensity from the fundamental, not visible anymore, to the combination. Using instead the wave function coefficients as an indicator for the resonance helps identify the problem and properly treat it. To facilitate the identification of excessively large terms related to LAMs, no variational correction, which would introduce a mixing of the states, was applied, so the IDVPT2 energies were used. Using these guidelines, the anharmonic force field was checked and normal modes related to force constants with absolute reduced values greater than 500 cm^{-1} and more than 80% of the harmonic frequencies were flagged as possible LAMs and checked. Four modes were selected and confirmed to be LAMs, corresponding to the rotations of the cyclopentadienyl ligand and of the three methyl groups on the phosphine. The modes were set as passive. The IDVPT2 calculations with the complete set of normal modes (NMs) showed five transitions whose energy increased after anharmonic correction. Among these modes, only two were identified as LAMs, the others were affected by unreliable force field elements and corrected once the LAMs were removed.

The final GVPT2 spectra without LAMs are displayed in the bottom panels of Figs. 3 and 4. Starker differences appear among the functionals, even in the mid-IR absorption spectrum. In particular, M06-2X predicts a strong enhancement of the peak at 1300 cm^{-1}, and ωB97X-D a triplet in the 1500–1200 cm^{-1} region, while the others show 2 broader bands of relatively comparable heights, quite similar to the harmonic level. The peculiar behavior of these two functionals is also visible in the mid-IR VCD spectrum (bottom right panel of Fig. 3). M06-2X predicts a '−,+' pattern at about 1400 cm^{-1}, at variance with all other functionals, and some relatively intense features in the 1400–1200 cm^{-1} region. The enhancement is even more marked for ωB97X-D, with 3 intense bands in that region. The VCD spectrum at this level even exhibits a very strong negative band at 1000 cm^{-1}.

While it would at first seem likely related to an overlooked resonance, an analysis of the cubic force constants (Fig. 5) shows unusual

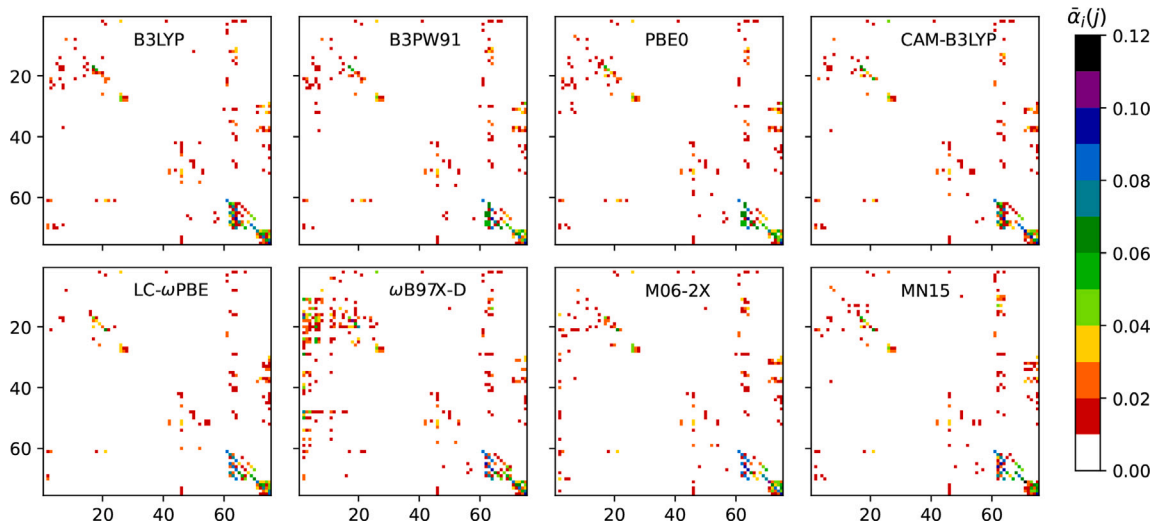

Fig. 5. Plot of $\tilde{\alpha}_i(j)$ for a selection of exchange–correlation functionals. A color code is used to show the magnitude of each term. The (x, y) coordinates in the plots correspond to the indexes of the normal modes sorted by increasing frequency (1 for the lowest).

couplings compared to the other functionals, hinting instead at a poor description of the anharmonic PES, in line with previous observations [64]. Other functionals also show interesting changes from the harmonic level. The single harmonic band at 1400 cm^{-1} is neatly split into 2 peaks with MN15, and a prominent shoulder with LC-ωPBE. The same band is significantly enhanced with PBE0, and instead broadened for B3PW91 and in a lesser extent B3LYP. Since the region is not expected to be dominated by strong anharmonic effects, CAM-B3LYP, as well as B3LYP, seems to be the most consistent. In the CH-stretching region (bottom panels of Fig. 4), the poor reliability of ωB97X-D and M06-2X is confirmed. The IR spectrum with LC-ωPBE, weak at the harmonic level, is enhanced and the dissymmetry in the intensity of the two main bands predicted by most functionals is recovered. However, the VCD spectrum shows blue-shifted intense features with a strong positive band at about 3000 cm^{-1}, which contrasts with the other functionals. This confirms the observations made in the mid-IR region, and the unsuitability of LC-ωPBE to predict the chiroptical response of this system. The other functionals generally show a relatively consistent behavior. The weak '−,+' pattern observed at about 2950–2920 cm^{-1} becomes a unique positive band of medium intensity with B3PW91, which could be caused by small differences in the harmonic energies, causing a redistribution of the intensities. Such behavior of this functional has been previously observed for medium-size systems [36].

Using B3LYP as reference, we now look at the contributions of the anharmonicity to the IR and VCD spectra. To this end, the spectra were also plotted by considering selectively only one type of anharmonicity at a time, related to the wave function (mechanical) or the property (electrical). It should be noted that in both cases, the mixed term vanishes by definition. The spectra are shown in Fig. 6, together with the pure harmonic ones, whose energies were scaled using a factor of 0.95 in the CH stretching region and 0.98 otherwise. First of all, it is noteworthy that the intensity of the CO stretching band, both in IR and VCD, is barely affected by anharmonicity. The use of the scaling factor causes a slight overestimation of the correction to the band position. A direct consequence is that the convergence on the intensity with the reduced-dimensionality scheme is expected to be very fast, so the energy should be the primary concern. In these conditions, the parameter $\tilde{\alpha}_i(j)$ should be sufficient to build efficiently the reduced-dimensionality scheme.

Turning to the fingerprint region, two regions can be defined, one dominated by fundamental bands, below 1500 cm^{-1}, and one populated by non-fundamental transitions between 1500 and 1900 cm^{-1}. The IR spectrum in the lower-energy part is virtually the same at the harmonic and anharmonic levels, except for a small energy shift above 1400 cm^{-1}. The VCD spectrum shows more variations. While the sign sequence is mostly preserved compared to the harmonic level, with a few minor changes, the intensities of the anharmonic bands are lower. To understand better the different contributions to the transition moments, the latter have been divided in 4 terms, harmonic, pure mechanical, pure electrical, and mixed terms. On this basis, the intensities were computed by setting all terms except one to zero. The resulting spectra are plotted in Fig. **S3** in the Supplementary Material. The variational correction was systematically ignored to facilitate the analysis. Looking more closely to the individual contributions, the mixed term, which only appears in fundamentals, is negligible in the fingerprint region. While still relatively weak, the pure electrical and mechanical anharmonicities shows more interesting features, especially around 1000 cm^{-1} and above 1350 cm^{-1}. By separating fundamentals and non-fundamentals bands (Fig. **S4** in the Supplementary Material), we can see that the stronger effects are on the latter. This means that the changes in the band patterns observed in the total anharmonic spectra in Fig. 6 are primarily caused by a redistribution of the intensities through the variational treatment. This is confirmed when looking at the total IDVPT2 spectrum in Fig. **S3** in the Supplementary Material, closer to the harmonic one. Interestingly, the spectrum with only the harmonic term and mechanical anharmonicity is superimposed with the total one, while the inclusion of pure electrical anharmonicity instead leads to stronger bands at 1000 and 1450 cm^{-1}. The effect of the electrical anharmonicity is thus in some way counterbalanced when including all anharmonic effects. Conversely, the higher-energy part of the fingerprint region, which consists purely of non-fundamental bands, is dominated by the electrical anharmonicity, while the mechanical anharmonicity is negligible.

A distinct picture emerges for the CH-stretching region. The band-shapes remain dominated by fundamental transitions like in the CO stretching region and the lower-energy part of the fingerprint region, but strong differences appear between the harmonic and anharmonic spectra for both IR and VCD. A comparison of the IDVPT2 (Fig. **S3** in the Supplementary Material) and GVPT2 (Fig. 6) shows an important impact of the variational correction on the final band-shape, in particular VCD, including on the band positions. Contrary to what is observed in the rest of the spectra, no single contribution, either mechanical or electrical, is sufficient to obtain the total spectra. For IR, the contribution from the electrical anharmonicity is rather small while the mixed term becomes non-negligible. The mixing of states introduced by the variational correction causes a shift in energy, with the two

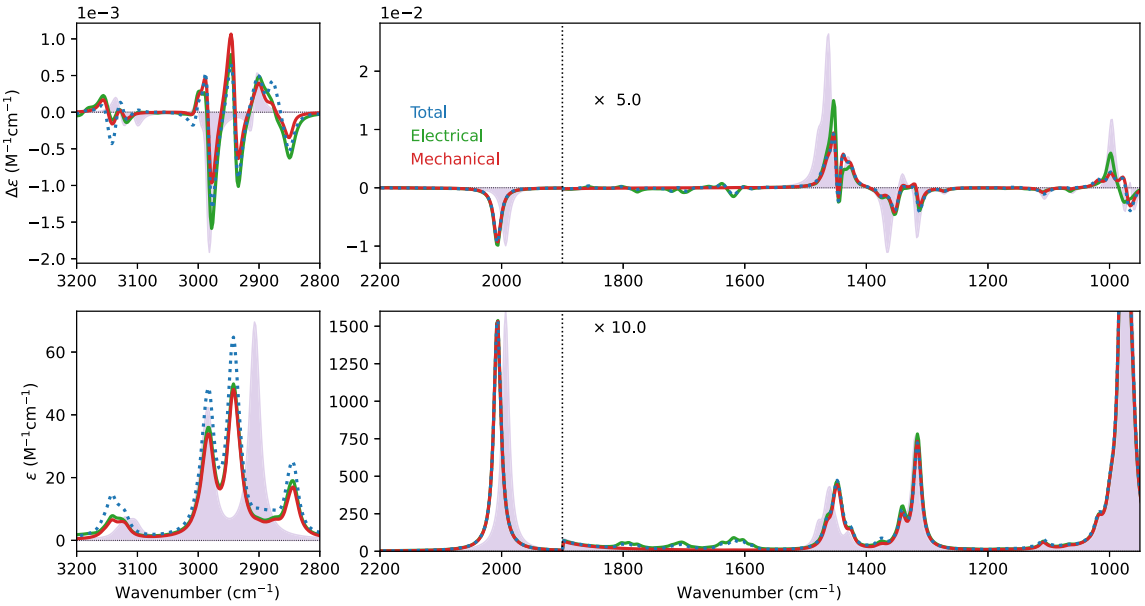

Fig. 6. Theoretical absorption and VCD spectra at the GVPT2 level in the CH stretching (left panels), CO stretching and mid-IR (right) regions of the template. The spectra calculated through evaluation of electrical (solid green lines) and mechanical (solid red lines) anharmonicities are reported separately and combined ("Total", dotted blue lines). The harmonic results are also reported as purple shades. Lorentzian broadening functions with half-widths at half-maximum of 10, 7 and 7 cm^{-1} were used in the CH-stretching, CO-stretching and mid-IR ranges, respectively. The intensity of the band-shape in the fingerprint region was enhanced tenfold to be more visible. Scaling factors of 0.95 and 0.98 were applied to harmonic wavenumbers in CH-stretching and mid-IR range, respectively.

bands within 3000–2900 cm^{-1} getting closer, and a redistribution of the intensities. The result is an enhancement of all band intensities in the region. For VCD, the mixed, electrical and mechanical terms give contributions of similar magnitudes. This is already visible on the band-shape at the IDVPT2 level in the 3000–2850 cm^{-1} region. Upon application of the variational correction, even the sign pattern changes, with a '+, −, +, −, +, −' alternation of intense bands.

This preliminary study on the full-dimensional system shows that, depending on the region of interest, different terms will dominate and that both electrical and mechanical anharmonicities are important to get a complete spectrum. The second important aspect is that the variational correction has a large effect on the overall band-shape, which further complicates the analysis of the contributions. For this reason, and keeping in mind the problem of the variational treatment with inactive modes, the analysis of the reduced-dimensionality schemes, their applicability and reliability will be done primarily with IDVPT2.

4.2. Reduced-dimensionality (RD) scheme on the template molecule

The main interest of reduced-dimensionality schemes is to improve the accuracy in the position and intensity of specific bands over the harmonic approximation by including the leading anharmonic effects without the need to compute the full set of anharmonic constants. This way, the overall computational cost can be kept under control. In the best conditions, this is achieved without any visible impact on the energies and intensities compared to the full calculation.

Typically, the target will be specific bands, generally fundamental states associated to some probe vibrations, like a C=O stretching, or a narrow region of the spectrum. In the latter case, a list of states need to be built, using for instance the scaled harmonic frequencies to build an initial set, which can be successively refined based on the corrected energies. For the sake of simplicity, we will consider a single state. The extension to a group of states is straightforward. For energies, since VPT2 requires only one formula, the discussion below can be easily transferred to any transition of interest. For the intensities, while the equations depend on the type of transition, a reduced-dimensionality model has no impact on first overtones and '1+1' combinations provided the concerned modes are active as defined in the theoretical background presented above. 3-quanta transitions have notably low intensities and could be discernible only in regions of the spectrum not of interest in the present work [35,37]. As a consequence, the focus will be in the present analysis on fundamental bands.

Considering the full anharmonic spectra, 4 fundamental bands lying in different regions of the spectrum were chosen to check the RD procedure. From low to high wavenumbers, they are a bending mode of Ru-CO (NM 22), the symmetric bending mode of CH_3 δ_{sym} (NM 48), the stretching mode of the coordinated CO ligand at about 2000 cm^{-1} (NM 61) and an anti-symmetric stretching mode of the methyl groups (NM 66). All of them have relatively intense signals in IR, VCD or both, thus making them appropriate targets. In Fig. 7, the convergence of the vibrational energies, dipole strengths (DS) and rotatory strengths (RS) against the number of NMs set active are reported. As discussed in the theoretical part, since we have a clear indicator to assess the impact of RD on the energy, for each active mode i corresponding to the selected fundamental state, we sorted the NMs j by decreasing values of $\bar{\alpha}_i(j)$. As can be observed from the left panels in Fig. 7, energies converge fast. With less than 10 NMs added to the list of active modes, all four vibration energies reach absolute errors with respect to the full anharmonic calculation within 2 cm^{-1}. The case of the CO stretching is singular, with the energy being almost at convergence with only mode 61 set active, thus confirming the extremely localized nature of the vibration.

For a better comparison, the values of $\bar{\alpha}_i(j)$ are also plotted in the same panels. All the curves show a clear change in their slope, therefore suggesting the use of the "knee" of the curve as heuristic to determine the number of NMs to be included in scheme.

Despite the dependence on the coordinates scales, this type of heuristic is commonly used in optimization problems, where the bend point represents the point beyond which the additional cost is no longer balanced by sensible improvements. Under the name of *elbow method*, it is commonly used in cluster analysis to determine the number of clusters in a data set [81].

For three out of the four vibrations, the point where the curve bends coincides with energy values at convergence. Let us consider

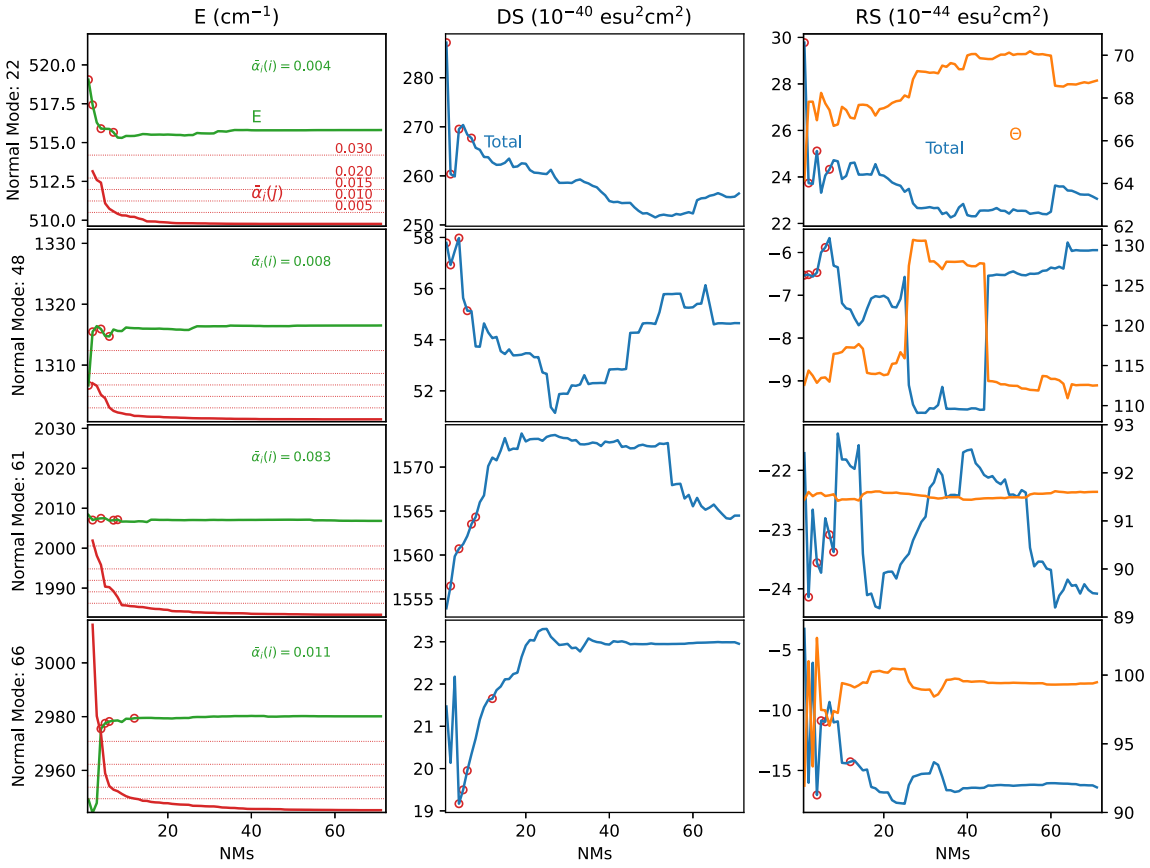

Fig. 7. Convergence plots of the energy (E), dipole strength (DS) and rotatory strength (RS) with respect to the number of normal modes (NMs) included in the RD scheme for i = 22,48,61,66 (see text). For each fundamental state $|1_i\rangle$, NMs were sorted by decreasing values of $\bar{\alpha}_i(j)$. The modes are then progressively added to the list of active modes (see Section 2). In the left panels, the $\bar{\alpha}_i(j)$ values are reported together with five threshold values. In the central and right panels, the last NM included at each threshold is marked with red circles. In the right column panels, in orange, we report also the angle between the electric and the magnetic dipole transition moments.

now the diagonal term, $\bar{\alpha}_i(i)$. For νCO, it is almost three times bigger than the second highest value of $\bar{\alpha}_i(j)$, which places this element well before the "knee". Interestingly, all values $\bar{\alpha}_i(i)$ (reported textually in the panels) have values close to the point where slopes change, suggesting that $\bar{\alpha}_i(i)$ could be used as a threshold whenever it is not null. In all cases, a threshold value of 0.01 gives results close to the full-dimensional one, with a limited increase of the computational cost over the harmonic level, while a more conservative value of 0.005 ensures energy convergence within 1 cm^{-1} (see Tab. **S1** in the Supplementary Material for numerical values at different thresholds).

The convergence for the intensities is analyzed in the central and right panels of Fig. 7. As expected from the theory, no obvious pattern can be isolated. After adding a few NMs as done for the energy, the full-dimensional anharmonic values seem to be reached. However, the further inclusion of modes leads to some instability with changes in RS and DS up to 60%. This type of behavior may have tremendous impacts on a sensitive spectroscopy like VCD. On the other hand, it is important to keep in mind that RD schemes are primarily intended for well-defined bands in the vibrational spectra, and so limit cases involving nearly perpendicular transition moments which could easily oscillate between positive and negative values would be less likely to meet this condition. Nevertheless, the evaluation of the convergence in the transition moments remains a difficult task, due to the presence of different contributions and the lack of a unique gauge, like $\bar{\alpha}_i(j)$ for the energy. To attempt a rationalization of the results, we report in Fig. **S5** in the Supplementary Material the contributions of the electrical, mechanical and mixed terms to the anharmonic correction to the intensities, as well as the values of $\bar{\alpha}_i(j)$, $\bar{\alpha}_i^M(k)$ and $|\mathbf{P}_{jji}/\mathbf{P}_i|$ for the transition moments of both electric and magnetic dipoles. This is completed by the representation of $\bar{\alpha}_i^E(i)$ and the whole $\bar{\alpha}_i^M(k)$ matrices in Fig. **S6** in the Supplementary Material. In agreement with the observations made on the contributions from the full set of anharmonic constants, a first consideration from the inspection of $\bar{\alpha}_i^E(i)$ is that the pure electrical anharmonicity has little effect on the fundamental intensities of the selected modes. In fact, the central and right panels of Fig. **S5** confirm that most of the variability can be related to the mechanical term.

Evaluating the potential impact of missing elements in the terms related to the mechanical anharmonicity (Eq. (13)) is not obvious. Most of the missing correction is expected to be related to potential 1-1 Darling–Dennison resonances as already explained in the theory. While resonance tests could be used, they may not be reliable due to the missing terms. In our case, the analysis of the evolution of the 1-1 DDRs patterns as functions of the modes included in the RD scheme reveal that, with a limited number of NMs included, all the 1-1 DDRs were correctly identified. Hence, a good strategy would be to first reach convergence on the energy and then to check if all modes involved in 1-1 DDRs related to the states of interest have been set active. If not, they should be added to converge faster on intensities. In this regard, the case of NM 66 is exemplary. While lowering κ_E improves the energy, the dipole strength is barely affected. On the other hand, the rotatory strength is heavily impacted. The RS goes from being slightly above the reference value to being underestimated by more than 30%. An analysis of the 1-1 DDRs shows that some modes involved in 1-1 DDRs were set active only after significantly lowering the threshold for $\bar{\alpha}_i(j)$. Including them earlier improves sensibly the convergence of RS (see the results reported in Tabs. **S1** and **S2** in the Supplementary Material).

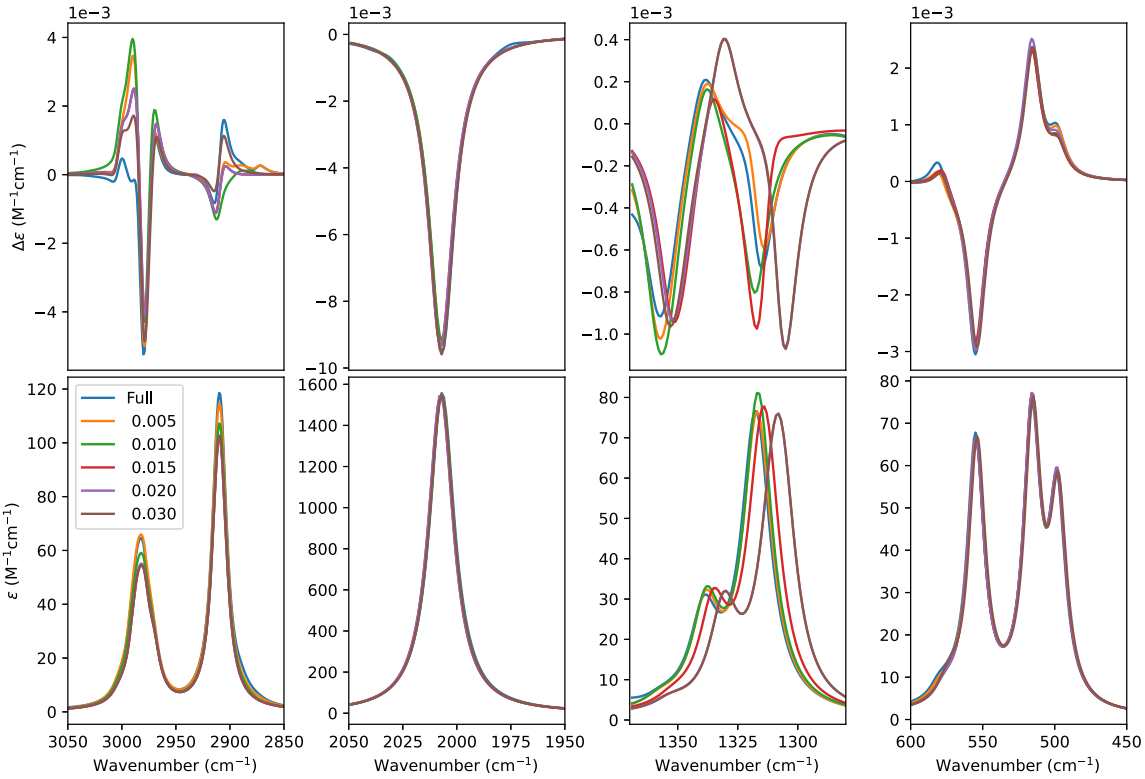

Fig. 8. Theoretical absorption and VCD spectra of the template in four target spectral ranges. The results obtained with the full anharmonic treatment are reported with results obtained employing different thresholds for $\tilde{\alpha}_i(j)$ to define the set of active modes (see text).

Interpreting the dependence of the intensities on the number of active modes once energy has converged is less trivial for the fundamentals of modes 48 and 61, but is a perfect illustration of the problems that arise from using a unique criterion to select the active modes in order to reproduce the spectral band-shape. Indeed, the sharp variations in the dipole and rotatory strengths show that $\tilde{\alpha}_i(j)$ may be a poor indicator to assess the contribution of each mode to the mechanical anharmonicity. This suggests that one should proceed with caution when adding normal modes to the RD scheme without a solid protocol, and that a combination of multiple criteria, for instance $\tilde{\alpha}_i(j)$ and the 1-1 DDR test, is a better approach.

Within this last described protocol, the results obtained on the target vibrations in the RD scheme are in excellent agreement with the results obtained with the full anharmonic treatment and are summarized in Tab. **S1** in the Supplementary Material.

The next step was to extend the procedure to groups of states in the regions surrounding modes 22, 48, 61 and 66 discussed above. Four regions were investigated, 600–400 cm^{-1}, 1400–1250 cm^{-1}, 2050–1950 cm^{-1} and 3050–2850 cm^{-1}. Fundamental transitions were selected starting from the harmonic solutions after applying scaling factors (0.95 in the CH stretching region, 0.98 in the CO stretching and mid-IR regions, and no scaling factor below 900 cm^{-1}) and on each mode the procedure described just above was applied to select coupled modes with five different thresholds for $\tilde{\alpha}_i(j)$. The subsets of active modes were then completed by including those involved in the non-fundamental transitions present in the selected ranges. Details on the NMs included for the four regions at different threshold values for $\tilde{\alpha}_i(j)$ are reported in Tab. **S4** in Supplementary Material and the resulting spectral band-shapes plotted in Fig. 8. Frequency ranges will generally include all resonant states that are likely to give the largest contributions. Hence, consistent subsets of active modes can be more directly built, and the number of normal modes to be added later will be limited. Minimizing the couplings between modes, through localization algorithms [82] or the use of special coordinates like internal coordinates [83] should in principle further reduce the subsets.

Proceeding to the analysis of the results from low to high wavenumbers, the first region is characterized by three intense features, which are observed in both absorption and VCD spectra and correspond to different bending modes of the RuCO moiety of the complex. These modes are well localized and are mostly coupled to one another. The only exception, as expected, is a strong coupling with the stretching mode of the CO ligand. In these conditions, the minimal set of NMs results based on the states identified in the region already leads to excellent agreement with the anharmonic calculation on the full system for both energies and intensities. For the latter, this is likely connected to the limited number of overall transitions in the regions, which means less potential resonances.

The next panels report a small portion of the fingerprint region, making it the first real challenge is this analysis. Nearby transitions can have a significant impact on the target ones, both in terms of energy and intensity. The result with the highest threshold is very poor, with large errors in the predicted transition energies. A possible consequence for a systems with a higher density of states like the real ruthenium complex could be incorrect assignments of the observed peaks. Lowering the threshold expands the network of active modes up to a maximum of 20 active NMs for $\kappa_E = 0.005$. Normal modes coupled through 1-1 DDRs are added early, already with a threshold value of 0.01, ensuring a good convergence in terms of energy and intensity.

The next region is characterized by the presence of the stretching of the CO ligand, which represents the best-case scenario for a RD anharmonic calculation. Indeed, it is the only fundamental transition in the region with a high intensity in both IR absorption and VCD. Moreover, the bulk of the anharmonic correction is fully contained in the terms directly connected to the mode, so excellent agreement with the full anharmonic spectra is reached by having a single active mode. Hence, the only real difficulty here lies in the subtlety of the

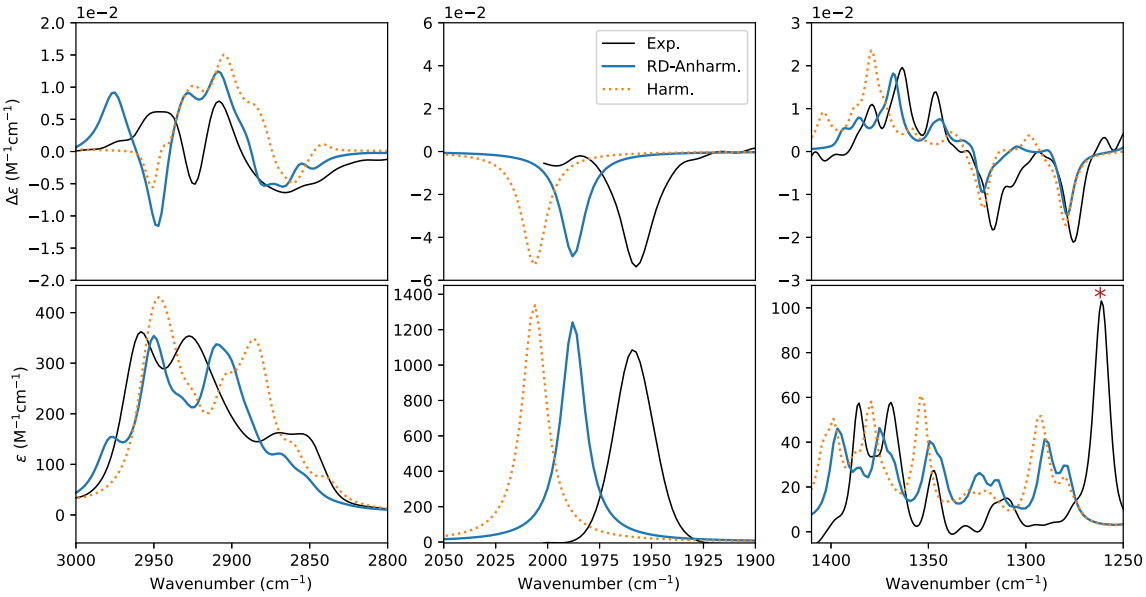

Fig. 9. Comparison of the experimental (black) IR (lower panels) and VCD (top panels) spectra of the *R*-**RuCl** with the corresponding harmonic (dashed orange) and RD anharmonic (blue) spectra. Theoretical spectra were simulated by assigning Lorentzian distribution functions with 5, 7 and 10 cm^{-1} of half-width at half-maximum from the left to the right panels, respectively. Scaling factors of 0.95 and 0.97 were applied to harmonic wavenumbers in the CH and mid-range regions, respectively. No scaling factor was used in the 2050–1900 cm^{-1} range. To facilitate the comparison in the narrow portion of the fingerprint region, a scaling factor of 0.99 was also applied to the RD anharmonic calculations (see text for details). The signal at about 1255 cm^{-1} marked with a red star is due to polysiloxane impurities in the sample.

resonance pattern, which primarily affects the intensity, thus causing their redistribution. If properly handled, two-quanta transitions have negligible intensities, which also helps to quickly reach convergence.

The last examined region covers the CH-stretching fundamental transitions, where the harmonic approximation is notoriously insufficient for the correct interpretation of the results [35]. At the anharmonic level, the presence of several two-quanta transitions may heavily impact the spectral band-shape and makes the simulation of this region arduous. A proper identification and treatment of resonances is a prerequisite to reliable simulations. For this simple template molecule, contributions from two-quanta transitions are limited, but their relevance grows quickly with the dimension of the system. Focusing on IR absorption first, the smallest subset of NMs, which by definition already includes all the CH-stretching transitions, is capable of reproducing well the positions of the most prominent bands. Analysis of the resonances reveals that all modes involved in 1-1 DDRs are already included. Consequently, and as expected from the results of NM 66, this size is already sufficient to reach a good agreement in the IR intensity, and larger subsets of NMs improve only slightly the convergence. The trend for VCD is less straightforward. The results suggest that the smaller subset may provide acceptable results, even though discrepancies with the full simulations are observed. For instance, the intense positive band at about 3000 cm^{-1} is the result of two transitions, one of which changes sign with the anharmonic correction. This behavior is observed for all five reduced-dimensionality tested schemes. Nonetheless, this type of issues is generally related to transitions of small intensity, whose reliability has often been questioned from both experimental and the computational sides [84–86]. A second consideration regards the systems of interest and the objectives of reduced-dimensionality approaches. In larger molecules, such low-intensity bands are likely hidden by more intense transitions, consequently making it an unlikely ideal target for the type of approach described here. In general, in systems of the size of the model and therefore with only few transitions, a full anharmonic treatment should be obviously preferred.

4.3. Reduced-dimensionality scheme on the full system

Encouraged by these promising results, we investigated three regions of the IR and VCD spectra of the **RuCl** complex within the RD approach. For this purpose, in addition to the spectral ranges already reported in Ref. [47], we recorded also the CH-stretching region. The spectra of the two diastereomers are given in Fig. **S7** in the Supplementary Material. As already noted for the mid-IR spectra, the VCD spectra are dominated by signals from the methyl group, therefore showing little difference between the two diastereomers.

For our simulations, we selected three ranges: a narrow zone in the fingerprint region, whose VCD is characterized by five intense signals '+,+,+,–,–' from high to low wavenumbers, the coordinated CO-stretching region, and the CH stretching region, characteristic of aliphatic bonds. On the basis of the results obtained with the template molecule and considering the size of the target complex, we used a κ_E = 0.01 as threshold to build the RD model. Considering the resolution of the experimental spectra, we introduced a further approximation for the fingerprint region, by assuming that the contributions due to combinations and overtones are negligible (see Tab. **S5** in the Supplementary Material for the list of NMs included).

The whole system has 222 harmonic vibrations. Within the RD approach, only 36, 3 and 44 normal modes, respectively, were set active and treated anharmonically. Even if we consider all three regions together, thanks to the partial overlap in the NMs (for a total of 76 modes), the overall computational advantage would still be remarkable. The resulting experimental, harmonic and RD anharmonic spectra are reported in Fig. 9.

At first glance, we can see that the inclusion of the anharmonic correction clearly improves the agreement with experiment compared to the harmonic level. Looking at the regions in order of increasing energy, the positive triplet in the IR and VCD fingerprint region is better reproduced both in terms of relative band positions and intensities.

In the central panels, which shows the CO stretching region, no scaling factor was applied to the harmonic results to highlight the

anharmonic correction to the vibrational energy of about 20 cm^{-1}. Like the template system, little contributions were observed to the IR and VCD intensities and the harmonic results already fairly matches the experimental values. Nonetheless, this result suggests an intrinsic limitation of the level of electronic structure theory employed for the simulations, including the basis sets as well, which may be too small.

It is the CH-stretching region where anharmonic contributions are expected to have the greatest impact. The experimental spectra show in absorption two main peaks close in energy and two less intense peaks at approximately 2850 cm^{-1}. In VCD, from low to high wavenumbers, four bands of comparable intensity producing a '$-,+,-,+$' alternation in signs are observed. In particular the first negative band is quite broad, clearly resulting from more than one transition, probably including non-fundamental contributions. The harmonic results are in weak agreement with experiment. In absorption the energy difference between the two main peaks is overestimated, while the lower-energy broad peak is reduced to a weak shoulder. In VCD, the discrepancy compared to the experiment is dramatic, the bands are predicted to have '$+,-,+,-$' signs at the harmonic level, in disagreement with experiments, and the peaks have substantial differences in intensity among them. Anharmonic results show a clear improvement, getting closer to experiment. On a qualitative basis, the sign sequence in VCD is correctly reproduced, even if the central bands are predicted too broad. The IR spectrum is in good agreement, and the shoulder at 2850 cm^{-1} is more pronounced than at the harmonic level, even if it remains underestimated compared to experiment.

Overall, these results are encouraging and can be further improved by adding more active modes. The protocol presented here offers robust non-empirical strategies to choose the extent of the reduced-dimensionality scheme by providing criteria to choose the sets of active modes based on the quantities to improve. Obviously, like with full-dimensionality VPT2, accuracy depends directly on the quality of the harmonic approximation, and intrinsically the chosen underlying electronic structure calculation method. This aspect was treated only cursorily, and a more systematic investigation is beyond the scope of the present study.

5. Conclusion

In this work, we have presented a methodology to extend VPT2 anharmonic calculations to cases where the generation of all necessary anharmonic constants would be too expensive. The approach, called reduced-dimensionality scheme, is based on a small selection of normal modes treated at the anharmonic level, and the rest within the harmonic approximation.

In order to evaluate *a priori* the impact of such an approach on the anharmonic spectra, starting from the formal VPT2 equations, we proposed four indicators, one for the energy and three for the properties. Using a smaller template system of the target ruthenium complex under investigation, we first showed how the quality of the anharmonic results is inherently influenced by the electronic structure calculations. This aspect is critical when considering the use of anharmonicity and naturally reduced-dimensionality schemes. Indeed, the latter is likely to introduce some degree of approximation, which may cumulate with the inherent limitations of DFT functionals and produce unreliable results. For chiroptical spectroscopy, we found that, among the functionals tested, LC-ωPBE is particularly ill-suited for predicting the spectrum of this system and ωB97X-D presented an artificially high coupling between modes in the VPT2 treatment, excluding them from any consideration for the RD scheme. On the other hand, the widely employed B3LYP and CAM-B3LYP functionals provided more consistent results in line with the other tested functionals.

Once defined the reference level of theory, the reduced-dimensionality scheme was validated first on the template system. We started by analyzing the convergence of the energy for target transitions (fundamentals of modes 22, 48, 61, 66). The dimensionless indicator $\bar{\alpha}_i(j)$ was used to sort the coupling of the other normal modes with respect to each active i normal modes in the system. Among the different tested thresholds, a value of "0.01" has proved to be a good compromise between computational cost and accuracy. The convergence on the transition moments and intensities, especially for fundamentals, as anticipated in the theoretical section from an analysis of the formulas, was less straightforward. We found that the inclusion of normal modes coupled with those of interest through 1-1 DDRs was crucial to reach convergence faster. Even though, in the RD scheme, the anharmonic corrections are truncated also for the resonances tests, all 1-1 DDRs involving the target fundamentals were correctly identified even with a minimal set of normal modes.

Working on full ranges, instead of single transitions, simplifies the task and may be simpler to carry out since almost all resonant states which are expected to give the largest contributions are automatically included. Starting from the harmonic transitions falling in the range of interest, $\bar{\alpha}_i(j)$ is sufficient to select the subset of normal modes to treat at the anharmonic level and to achieve a simulation of the spectra on par with the full VPT2 treatment.

The results obtained on the simulation of three ranges for the ruthenium complex confirmed the validity of the strategy proposed here. With these results, the procedure reported in this work paves the way for the investigation of large systems with the inclusion of leading anharmonic effects, generally excluded because of the total cost, even in spectroscopic ranges usually ignored and where anharmonicity plays a fundamental role.

These preliminary results are very encouraging and must be confirmed with other kinds of systems, including purely organic molecules. The possibility to define reliable thresholds would be the starting point towards automated or semi-automated protocols for an integration in black-box procedures, making such a scheme accessible to a broad community of scientists.

Dedication

We would like to thank Laurence A. Nafie for his pioneering work in VOA spectroscopy, both on the theoretical and experimental aspects of the techniques, which have been a source of inspiration for many of us, and has played a fundamental role in a field that has become the center of our research. We would also like to thank him for his kindness and his availability, his advice having been a source of inspiration in several of our projects.

CRediT authorship contribution statement

Marco Fusè: Conceptualization, Data curation, Funding acquisition, Investigation, Methodology, Visualization, Writing – original draft, Writing – review & editing. **Giuseppe Mazzeo:** Investigation, Writing – original draft, Writing – review & editing. **Giovanna Longhi:** Funding acquisition, Writing – original draft, Writing – review & editing. **Sergio Abbate:** Writing – original draft, Writing – review & editing. **Qin Yang:** Writing – original draft. **Julien Bloino:** Conceptualization, Funding acquisition, Methodology, Software, Supervision, Visualization, Writing – original draft, Writing – review & editing.

Declaration of competing interest

The authors declare the following financial interests/personal relationships which may be considered as potential competing interests: Julien Bloino reports financial support was provided by Italian Ministry of University and Research. Giovanna Longhi reports financial support was provided by Italian Ministry of University and Research.

Data availability

Data will be made available on request.

Acknowledgments

MF would like to thank professor Edoardo Cesarotti. The study of the chiral transition metal complexes that are investigated here began with him. Funding was provided by the Italian Ministry of University and Research (MUR) through the PRIN program (PRIN 2017, project "Physico-chemical Heuristic Approaches: Nanoscale Theory of Molecular Spectroscopy" (PHANTOMS), prot. 2017A4XRCA; PRIN 2020, project "Photoreactive Systems upon Irradiation: Modelling and Observation of Vibrational Interactions with the Environment" (PSI-MOVIE), prot. 2020HTSXMA; PRIN 2022, project "Enhancing Circularly Polarised Emitters Quantum Efficiency Exploiting Singlet-Triplet Inversion" (INVESTCPE), prot. 2022CXHY3 A). Computing facilities from SNS HPC are acknowledged.

Appendix A. Supplementary data

Complement to the theoretical background; Additional figures and tables; experimental procedure and VCD spectra in CH-region for both the diastereomers; molecular geometries in XYZ format.

Supplementary material related to this article can be found online at https://doi.org/10.1016/j.saa.2024.123969.

References

[1] L.A. Nafie, Vibrational Optical Activity: Principles and Applications, John Wiley & Sons, Chichester, UK, 2011.
[2] P. Polavarapu, Chiroptical Spectroscopy: Fundamentals and Applications, CRC Press LLC, 2019.
[3] T.A. Keiderling, Structure of condensed phase peptides: Insights from vibrational circular dichroism and raman optical activity techniques, Chem. Rev. 120 (7) (2020) 3381–3419, http://dx.doi.org/10.1021/acs.chemrev.9b00636.
[4] V. Parchaňský, J. Kapitán, P. Bouř, Inspecting chiral molecules by raman optical activity spectroscopy, RSC Adv. 4 (2014) 57125–57136, http://dx.doi.org/10.1039/C4RA10416A.
[5] G. Mazzeo, A. Cimmino, M. Masi, G. Longhi, L. Maddau, M. Memo, A. Evidente, S. Abbate, Importance and difficulties in the use of chiroptical methods to assign the absolute configuration of natural products: The case of phytotoxic pyrones and furanones produced by diplodia corticola, J. Nat. Prod. 80 (9) (2017) 2406–2415, http://dx.doi.org/10.1021/acs.jnatprod.7b00119.
[6] G. Mazzeo, G. Longhi, S. Abbate, F. Mangiavacchi, C. Santi, J. Han, V.A. Soloshonok, L. Melensi, R. Ruzziconi, Mannich-type addition of 1 , 3-dicarbonyl compounds to chiral tert-butanesulfinyltrifluoroacetaldimines. mechanistic aspects and chiroptical studies, Org. Biomol. Chem. 16 (2018) 8742–8750, http://dx.doi.org/10.1039/C8OB02204F.
[7] J.M. Batista Jr., V.d.S. Blanch, E.W. Bolzani, Recent advances in the use of vibrational chiroptical spectroscopic methods for stereochemical characterization of natural products, Nat. Prod. Rep. 32 (2015) 1280–1302, http://dx.doi.org/10.1039/C5NP00027K.
[8] B.R.P. Batista, M.E.D. Angrisani, S.M.P.D. Lima, V.H. Silva, H.A. Schettini, F.M.d. Chagas, A.N.L. Santos Jr., J.M. Batista Jr., A.L. Valverde, Absolute configuration reassignment of natural products: An overview of the last decade, J. Braz. Chem. Soc. 32 (8) (2021) 1499–1518, http://dx.doi.org/10.21577/0103-5053.20210079, J. Braz. Chem. Soc., 2021 32(8).
[9] P.L. Polavarapu, E. Santoro, Vibrational optical activity for structural characterization of natural products, Nat. Prod. Rep. 37 (2020) 1661–1699, http://dx.doi.org/10.1039/D0NP00025F.
[10] E. Burgueño-Tapia, P. Joseph-Nathan, Vibrational circular dichroism: recent advances for the assignment of the absolute configuration of natural products, Nat. Prod. Commun. 12 (5) (2017) 1934578X1701200501.
[11] F. Mangiavacchi, G. Mazzeo, M.C. Graziani, F. Marini, J. Drabowicz, E. Wielgus, L. Sancineto, G. Longhi, R. Vivani, S. Abbate, C. Santi, Vibrational and electronic circular dichroism study of chiral seleno compounds prepared from a naphthol based diselenide, Eur. J. Organic Chem. 2022 (23) (2022) e202200282, http://dx.doi.org/10.1002/ejoc.202200282, arXiv:https://chemistry-europe.onlinelibrary.wiley.com/doi/pdf/10.1002/ejoc.202200282 URL https://chemistry-europe.onlinelibrary.wiley.com/doi/abs/10.1002/ejoc.202200282.
[12] M.A.J. Koenis, Y. Xia, S.R. Domingos, L. Visscher, W.J. Buma, V.P. Nicu, Taming conformational heterogeneity in and with vibrational circular dichroism spectroscopy, Chem. Sci. 10 (2019) 7680–7689, http://dx.doi.org/10.1039/C9SC02866H.
[13] C. Merten, V. Smyrniotopoulos, D. Tasdemir, Assignment of absolute configurations of highly flexible linear diterpenes from the brown alga bifurcaria bifurcata by vcd spectroscopy, Chem. Commun. 51 (2015) 16217–16220, http://dx.doi.org/10.1039/C5CC05659D.
[14] M.A.J. Koenis, C.S. Chibueze, M.A. Jinks, V.P. Nicu, L. Visscher, S.M. Goldup, W.J. Buma, Vibrational circular dichroism spectroscopy for probing the expression of chirality in mechanically planar chiral rotaxanes, Chem. Sci. 11 (2020) 8469–8475, http://dx.doi.org/10.1039/D0SC02485F.
[15] A.-C. Chamayou, S. Lüdeke, V. Brecht, T.B. Freedman, L.A. Nafie, C. Janiak, Chirality and diastereoselection of δ/λ-configured tetrahedral zinc complexes through enantiopure schiff base complexes: Combined vibrational circular dichroism, density functional theory, 1h nmr, and x-ray structural studies, Inorg. Chem. 50 (22) (2011) 11363–11374, http://dx.doi.org/10.1021/ic2009557.
[16] D.A. Young, T.B. Freedman, E.D. Lipp, L.A. Nafie, Vibrational circular dichroism in transition-metal complexes. 2. ion association, ring conformation, and ring currents of ethylenediamine ligands, J. Am. Chem. Soc. 108 (23) (1986) 7255–7263, http://dx.doi.org/10.1021/ja00283a021.
[17] M.R. Poopari, Z. Dezhahang, Y. Xu, A comparative vcd study of methyl mandelate in methanol, dimethyl sulfoxide URL , and chloroform: explicit and implicit solvation models, Phys. Chem. Chem. Phys. 15 (2013) 1655–1665, http://dx.doi.org/10.1039/C2CP42722B.
[18] S. Ghidinelli, S. Abbate, J. Koshoubu, Y. Araki, T. Wada, G. Longhi, Solvent effects and aggregation phenomena studied by vibrational optical activity and molecular dynamics: The case of pantolactone, J. Phys. Chem. B 124 (22) (2020) 4512–4526, http://dx.doi.org/10.1021/acs.jpcb.0c01483.
[19] L. Weirich, K. Blanke, C. Merten, More complex, less complicated? explicit solvation of hydroxyl groups for the analysis of vcd spectra, Phys. Chem. Chem. Phys. 22 (2020) 12515–12523, http://dx.doi.org/10.1039/D0CP01656J.
[20] T.A. Keiderling, Protein and peptide secondary structure and conformational determination with vibrational circular dichroism, Curr. Opin. Chem. Biol. 6 (5) (2002) 682–688, http://dx.doi.org/10.1016/S1367-5931(02)00369-1, URL https://www.sciencedirect.com/science/article/pii/S1367593102003691.
[21] T.A. Keiderling, Vibrational circular dichroism of peptides and proteins: survey of techniques, qualitative and quantitative analyses, and applications, Infr. Raman Spectr. Biol. Mater. (2001) 55–100.
[22] R. Schweitzer-Stenner, F. Eker, K. Griebenow, X. Cao, L.A. Nafie, The conformation of tetraalanine in water determined by polarized raman, ft-ir, and vcd spectroscopy, J. Am. Chem. Soc. 126 (9) (2004) 2768–2776, http://dx.doi.org/10.1021/ja039452c.
[23] S.R. Domingos, A. Huerta-Viga, L. Baij, S. Amirjalayer, D.A.E. Dunnebier, A.J.C. Walters, M. Finger, L.A. Nafie, B. de Bruin, W.J. Buma, S. Woutersen, Amplified vibrational circular dichroism as a probe of local biomolecular structure, J. Am. Chem. Soc. 136 (9) (2014) 3530–3535, http://dx.doi.org/10.1021/ja411405s.
[24] S. Ma, X. Cao, M. Mak, A. Sadik, C. Walkner, T.B. Freedman, I.K. Lednev, R.K. Dukor, L.A. Nafie, Vibrational circular dichroism shows unusual sensitivity to protein fibril formation and development in solution, J. Am. Chem. Soc. 129 (41) (2007) 12364–12365, http://dx.doi.org/10.1021/ja074188z.
[25] D. Kurouski, R.A. Lombardi, R.K. Dukor, I.K. Lednev, L.A. Nafie, Direct observation and ph control of reversed supramolecular chirality in insulin fibrils by vibrational circular dichroism, Chem. Commun. 46 (2010) 7154–7156, http://dx.doi.org/10.1039/C0CC02423F.
[26] V. Andrushchenko, Z. Leonenko, D. Cramb, H. van de Sande, H. Wieser, Vibrational cd (vcd) and atomic force microscopy (afm) study of dna interaction with cr3+ ions: Vcd and afm evidence of dna condensation, Biopolymers 61 (4) (2001) 243–260, http://dx.doi.org/10.1002/bip.10159, arXiv:https://onlinelibrary.wiley.com/doi/pdf/10.1002/bip.10159 URL https://onlinelibrary.wiley.com/doi/abs/10.1002/bip.10159.
[27] M. Krupová, P. Leszczenko, E. Sierka, S. Emma Hamplová, R. Pelc, V. Andrushchenko, Vibrational circular dichroism unravels supramolecular chirality and hydration polymorphism of nucleoside crystals, Chem. – Eur. J. 28 (63) (2022) e202201922, http://dx.doi.org/10.1002/chem.202201922, arXiv:https://chemistry-europe.onlinelibrary.wiley.com/doi/pdf/10.1002/chem.202201922 URL https://chemistry-europe.onlinelibrary.wiley.com/doi/abs/10.1002/chem.202201922.
[28] C. Merten, Recent advances in the application of vibrational circular dichroism spectroscopy for the characterization of asymmetric catalysts, Eur. J. Organic Chem. 2020 (37) (2020) 5892–5900, http://dx.doi.org/10.1002/ejoc.202000876.
[29] T.P. Golub, A.H. Abazid, B.J. Nachtsheim, C. Merten, Structure elucidation of in situ generated chiral hypervalent iodine complexes via vibrational circular dichroism (vcd), Angew. Chem. Int. Ed. 61 (50) (2022) e202204624, http://dx.doi.org/10.1002/anie.202204624, arXiv:https://onlinelibrary.wiley.com/doi/pdf/10.1002/anie.202204624 URL https://onlinelibrary.wiley.com/doi/abs/10.1002/anie.202204624.
[30] M.A.J. Koenis, V.P. Nicu, L. Visscher, C. Kuehn, M. Bremer, M. Krier, H. Untenecker, U. Zhumaev, B. Küstner, W.J. Buma, Vibrational circular dichroism studies of exceptionally strong chirality inducers in liquid crystals, Phys. Chem. Chem. Phys. 23 (2021) 10021–10028, http://dx.doi.org/10.1039/D1CP00854D.
[31] T. Taniguchi, K. Monde, Exciton chirality method in vibrational circular dichroism, J. Am. Chem. Soc. 134 (8) (2012) 3695–3698, http://dx.doi.org/10.1021/ja3001584.
[32] G. Mazzeo, M. Fusè, G. Longhi, I. Rimoldi, E. Cesarotti, A. Crispini, S. Abbate, Vibrational circular dichroism and chiroptical properties of chiral ir(iii) luminescent complexes, Dalton Trans. 45 (2016) 992–999, http://dx.doi.org/10.1039/C5DT03642A.

[33] P. Stephens, F. Devlin, J. Cheeseman, VCD Spectroscopy for Organic Chemists, Taylor & Francis, 2012.

[34] N.M. Kreienborg, J. Bloino, T. Osowski, C.H. Pollok, C. Merten, The vibrational cd spectra of propylene oxide in liquid xenon: a proof-of-principle cryovcd study that challenges theory, Phys. Chem. Chem. Phys. 21 (2019) 6582–6587, http://dx.doi.org/10.1039/C9CP00537D.

[35] M. Fusè, G. Longhi, G. Mazzeo, S. Stranges, F. Leonelli, G. Aquila, E. Bodo, B. Brunetti, C. Bicchi, C. Cagliero, J. Bloino, S. Abbate, Anharmonic aspects in vibrational circular dichroism spectra from 900 to 9000 cm^{-1} for methyloxirane and methylthiirane, J. Phys. Chem. A 126 (38) (2022) 6719–6733, http://dx.doi.org/10.1021/acs.jpca.2c05332, arXiv:https://doi.org/10.1021/acs.jpca.2c05332.

[36] Q. Yang, J. Bloino, An effective and automated processing of resonances in vibrational perturbation theory applied to spectroscopy, J. Phys. Chem. A 126 (49) (2022) 9276–9302, http://dx.doi.org/10.1021/acs.jpca.2c06460, arXiv:https://doi.org/10.1021/acs.jpca.2c06460.

[37] Q. Yang, J. Kapitán, P. Bouř, J. Bloino, Anharmonic vibrational raman optical activity of methyloxirane: Theory and experiment pushed to the limits, J. Phys. Chem. Lett. 13 (38) (2022) 8888–8892, http://dx.doi.org/10.1021/acs.jpclett.2c02320.

[38] L.A. Nafie, Vibrational optical activity: From discovery and development to future challenges, Chirality 32 (5) (2020) 667–692, http://dx.doi.org/10.1002/chir.23191, arXiv:https://onlinelibrary.wiley.com/doi/pdf/10.1002/chir.23191 URL https://onlinelibrary.wiley.com/doi/abs/10.1002/chir.23191.

[39] H.H. Nielsen, The vibration–rotation energies of molecules, Rev. Modern Phys. 23 (2) (1951) 90–136, http://dx.doi.org/10.1103/RevModPhys.23.90, URL http://link.aps.org/doi/10.1103/RevModPhys.23.90.

[40] C. Puzzarini, J. Bloino, N. Tasinato, V. Barone, Accuracy and interpretability: The devil and the holy grail. new routes across old boundaries in computational spectroscopy, Chem. Rev. 119 (13) (2019) 8131–8191, http://dx.doi.org/10.1021/acs.chemrev.9b00007, arXiv:https://doi.org/10.1021/acs.chemrev.9b00007.

[41] M. Biczysko, J. Bloino, C. Puzzarini, Computational challenges in astrochemistry, Wiley Interdiscip. Rev.: Comput. Mol. Sci. 8 (3) (2018) e1349, http://dx.doi.org/10.1002/wcms.1349, URL https://onlinelibrary.wiley.com/doi/abs/10.1002/wcms.1349.

[42] K.B. Beć, C.W. Huck, Breakthrough potential in near-infrared spectroscopy: Spectra simulation. a review of recent developments, Front. Chem. 7 (2019) 48, http://dx.doi.org/10.3389/fchem.2019.00048, URL https://www.frontiersin.org/article/10.3389/fchem.2019.00048.

[43] V. Barone, G. Ceselin, M. Fusè, N. Tasinato, Accuracy meets interpretability for computational spectroscopy by means of hybrid and double-hybrid functionals, Front. Chem. 8 (2020) 859, http://dx.doi.org/10.3389/fchem.2020.584203, URL https://www.frontiersin.org/article/10.3389/fchem.2020.584203.

[44] P. Goel, J.F. Stanton, Semiclassical transition state theory based on fourth order vibrational perturbation theory: Model system studies beyond symmetric eckart barrier, J. Chem. Phys. 149 (13) (2018) 134109, http://dx.doi.org/10.1063/1.5040978.

[45] S.V. Krasnoshchekov, E.V. Isayeva, N.F. Stepanov, Numerical-analytic implementation of the higher-order canonical van vleck perturbation theory for the interpretation of medium-sized molecule vibrational spectra, J. Phys. Chem. A 116 (14) (2012) 3691–3709, http://dx.doi.org/10.1021/jp211400w, URL http://pubs.acs.org/doi/abs/10.1021/jp211400w.

[46] R. Franke, H. Müller, J. Noga, Static electrical response properties of F^-, ne, and hf using explicitly correlated r12 coupled cluster approach, J. Chem. Phys. 114 (18) (2001) 7746–7752, http://dx.doi.org/10.1063/1.1361249, URL http://scitation.aip.org/content/aip/journal/jcp/114/18/10.1063/1.1361249.

[47] M. Fusè, G. Mazzeo, G. Longhi, S. Abbate, D. Zerla, I. Rimoldi, A. Contini, E. Cesarotti, Vcd spectroscopy as an excellent probe of chiral metal complexes containing a carbon monoxide vibrational chromophore, Chem. Commun. 51 (2015) 9385–9387, http://dx.doi.org/10.1039/C5CC02170G.

[48] R. Noyori, Asymmetric catalysis: Science and opportunities (nobel lecture), Angew. Chem. Int. Ed. 41 (12) (2002) 2008–2022, http://dx.doi.org/10.1002/1521-3773(20020617)41:12<2008::AID-ANIE2008>3.0.CO;2-4.

[49] O. Pàmies, J.-E. Bäckvall, Combination of enzymes and metal catalysts. a powerful approach in asymmetric catalysis, Chem. Rev. 103 (8) (2003) 3247–3262, http://dx.doi.org/10.1021/cr020029g.

[50] S. Takahashi, J. Wang, D. Rousseau, K. Ishikawa, T. Yoshida, J. Host, M. Ikeda-Saito, Heme-heme oxygenase complex. structure of the catalytic site and its implication for oxygen activation., J. Biol. Chem. 269 (2) (1994) 1010–1014, http://dx.doi.org/10.1016/S0021-9258(17)42212-5.

[51] H. Brunner, Optically active organometallic compounds of transition elements with chiral metal atoms, Angew. Chem. Int. Ed. 38 (9) (1999) 1194–1208, http://dx.doi.org/10.1002/(SICI)1521-3773(19990503)38:9<1194::AID-ANIE1194>3.0.CO;2-X.

[52] A. Nakamura, T. Kageyama, H. Goto, B.P. Carrow, S. Ito, K. Nozaki, P-chiral phosphine–sulfonate/palladium-catalyzed asymmetric copolymerization of vinyl acetate with carbon monoxide, J. Am. Chem. Soc. 134 (30) (2012) 12366–12369, http://dx.doi.org/10.1021/ja3044344.

[53] L.J. Bellamy, The Infra-Red Spectra of Complex Molecules, vol. 1, Chapman and Hall London, 1975.

[54] M. Fusè, I. Rimoldi, E. Cesarotti, S. Rampino, V. Barone, On the relation between carbonyl stretching frequencies and the donor power of chelating diphosphines in nickel dicarbonyl complexes, Phys. Chem. Chem. Phys. 19 (2017) 9028–9038, http://dx.doi.org/10.1039/C7CP00982H.

[55] V. Barone, M. Biczysko, J. Bloino, M. Borkowska-Panek, I. Carnimeo, P. Panek, Toward anharmonic computations of vibrational spectra for large molecular systems, Int. J. Quantum Chem. 112 (9) (2012) 2185–2200, http://dx.doi.org/10.1002/qua.23224.

[56] J. Bloino, A vpt2 route to near-infrared spectroscopy: The role of mechanical and electrical anharmonicity, J. Phys. Chem. A 119 (21) (2015) 5269–5287, http://dx.doi.org/10.1021/jp509985u.

[57] J. Bloino, M. Biczysko, V. Barone, Anharmonic effects on vibrational spectra intensities: Infrared, raman, vibrational circular dichroism, and raman optical activity, J. Phys. Chem. A 119 (49) (2015) 11862–11874, http://dx.doi.org/10.1021/acs.jpca.5b10067.

[58] J. Bloino, V. Barone, A second-order perturbation theory route to vibrational averages and transition properties of molecules: General formulation and application to infrared and vibrational circular dichroism spectroscopies, J. Chem. Phys. 136 (12) (2012) 124108, http://dx.doi.org/10.1063/1.3695210, URL http://link.aip.org/link/?JCP/136/124108/1.

[59] S.V. Krasnoshchekov, E.V. Isayeva, N.F. Stepanov, Criteria for first- and second-order vibrational resonances and correct evaluation of the darling-dennison resonance coefficients using the canonical van vleck perturbation theory, J. Chem. Phys. 141 (23) (2014) 234114, http://dx.doi.org/10.1063/1.4903927, URL http://scitation.aip.org/content/aip/journal/jcp/141/23/10.1063/1.4903927.

[60] M.A. Boyer, A.B. McCoy, A wave function correction-based approach to the identification of resonances for vibrational perturbation theory, J. Chem. Phys. 157 (16) (2022) 164113, http://dx.doi.org/10.1063/5.0121915.

[61] A.M. Rosnik, W.F. Polik, Vpt2+k spectroscopic constants and matrix elements of the transformed vibrational hamiltonian of a polyatomic molecule with resonances using van vleck perturbation theory, Mol. Phys. 112 (2) (2014) 261–300, http://dx.doi.org/10.1080/00268976.2013.808386.

[62] J.M.L. Martin, T.J. Lee, P.M. Taylor, J.-P. François, The anharmonic force field of ethylene, c_2h_4, by means of accurate ab initio calculations, J. Chem. Phys. 103 (7) (1995) 2589–2602, http://dx.doi.org/10.1063/1.469681, martin test.

[63] V. Barone, Anharmonic vibrational properties by a fully automated second-order perturbative approach, J. Chem. Phys. 122 (1) (2005) 014108, http://dx.doi.org/10.1063/1.1824881, URL http://link.aip.org/link/?JCP/122/014108/1.

[64] J. Bloino, A. Baiardi, M. Biczysko, Aiming at an accurate prediction of vibrational and electronic spectra for medium-to-large molecules: An overview, Int. J. Quantum Chem. 116 (21) (2016) 1543–1574, http://dx.doi.org/10.1002/qua.25188.

[65] P.R. Franke, J.F. Stanton, G.E. Douberly, How to VPT2: Accurate and intuitive simulations of CH stretching infrared spectra using VPT2+K with large effective hamiltonian resonance treatments, J. Phys. Chem. A 125 (6) (2021) 1301–1324, http://dx.doi.org/10.1021/acs.jpca.0c09526, arXiv:https://doi.org/10.1021/acs.jpca.0c09526.

[66] B.T. Darling, D.M. Dennison, The water vapor molecule, Phys. Rev. 57 (2) (1940) 128–139, http://dx.doi.org/10.1103/PhysRev.57.128, URL http://link.aps.org/doi/10.1103/PhysRev.57.128.

[67] Double and triple-ζ basis sets of sns family, are available for download, 2011, [cited October, 6 2011]. URL https://smart.sns.it/?pag=download.

[68] P.J. Hay, W.R. Wadt, Ab initio effective core potentials for molecular calculations. Potentials for K to Au including the outermost core orbitals, J. Chem. Phys. 82 (1) (1985) 299–310, http://dx.doi.org/10.1063/1.448975.

[69] E. Cancès, B. Mennucci, J. Tomasi, A new integral equation formalism for the polarizable continuum model: Theoretical background and applications to isotropic and anisotropic dielectrics, J. Chem. Phys. 107 (8) (1997) 3032–3041, http://dx.doi.org/10.1063/1.474659, URL http://scitation.aip.org/content/aip/journal/jcp/107/8/10.1063/1.474659.

[70] G.W. Frisch, H.B. Trucks, G.E. Schlegel, M.A. Scuseria, J.R. Robb, G. Cheeseman, V. Scalmani, G.A. Barone, H. Petersson, X. Nakatsuji, M. Li, A.V. Caricato, J. Marenich, B.G. Bloino, R. Janesko, B. Gomperts, H.P. Mennucci, J.V. Hratchian, A.F. Ortiz, J.L. Izmaylov, D. Sonnenberg, F. Williams-Young, F. Ding, F. Lipparini, J. Egidi, B. Goings, A. Peng, T. Petrone, D. Henderson, V.G. Ranasinghe, J. Zakrzewski, N. Gao, G. Rega, W. Zheng, M. Liang, M. Hada, K. Ehara, R. Toyota, J. Fukuda, M. Hasegawa, T. Ishida, Y. Nakajima, O. Honda, H. Kitao, T. Nakai, K. Vreven, J.A. Throssell, M.J. Montgomery Jr., F. Peralta, M.J. Ogliaro, J.J. Bearpark, E.N. Heyd, K.N. Brothers, V.N. Kudin, T.A. Staroverov, R. Keith, J. Kobayashi, K. Normand, A.P. Raghavachari, J.C. Rendell, S.S. Burant, J. Iyengar, M. Tomasi, J.M. Cossi, M. Millam, C. Klene, R. Adamo, J.W. Cammi, R.L. Ochterski, K. Martin, O. Morokuma, J.B. Farkas, D.J. Foresman, J.E. Fox, Gaussian 16 Revision C.01, gaussian Inc., Wallingford CT, 2019.

[71] Q. Yang, M. Mendolicchio, V. Barone, J. Bloino, Accuracy and reliability in the simulation of vibrational spectra: A comprehensive benchmark of energies and intensities issuing from generalized vibrational perturbation theory to second order (GVPT2), Front. Astron. Space Sci. 8 (2021) 665232, http://dx.doi.org/10.3389/fspas.2021.665232, URL https://www.frontiersin.org/article/10.3389/fspas.2021.665232.

[72] A.D. Becke, Density-functional thermochemistry. III. The role of exact exchange, J. Chem. Phys. 98 (7) (1993) 5648–5652, http://dx.doi.org/10.1063/1.464913, arXiv:https://pubs.aip.org/aip/jcp/article-pdf/98/7/5648/11091662/5648_1_online.pdf.

[73] P.J. Stephens, F.J. Devlin, C.F. Chabalowski, M.J. Frisch, Ab initio calculation of vibrational absorption and circular dichroism spectra using density functional force fields, J. Phys. Chem. 98 (45) (1994) 11623–11627, http://dx.doi.org/10.1021/j100096a001.

[74] C. Adamo, V. Barone, Toward reliable density functional methods without adjustable parameters: The PBE0 model, J. Chem. Phys. 110 (13) (1999) 6158–6170, http://dx.doi.org/10.1063/1.478522, arXiv:https://pubs.aip.org/aip/jcp/article-pdf/110/13/6158/10797469/6158_1_online.pdf.

[75] T. Yanai, D.P. Tew, N.C. Handy, A new hybrid exchange–correlation functional using the coulomb-attenuating method (cam-b3lyp), Chem. Phys. Lett. 393 (1) (2004) 51–57, http://dx.doi.org/10.1016/j.cplett.2004.06.011, URL https://www.sciencedirect.com/science/article/pii/S0009261404008620.

[76] T.M. Henderson, A.F. Izmaylov, G. Scalmani, G.E. Scuseria, Can short-range hybrids describe long-range-dependent properties? J. Chem. Phys. 131 (4) (2009) 044108, http://dx.doi.org/10.1063/1.3185673, arXiv:https://pubs.aip.org/aip/jcp/article-pdf/doi/10.1063/1.3185673/15635537/044108_1_online.pdf.

[77] J.-D. Chai, M. Head-Gordon, Long-range corrected hybrid density functionals with damped atom–atom dispersion corrections, Phys. Chem. Chem. Phys. 10 (2008) 6615–6620, http://dx.doi.org/10.1039/B810189B.

[78] R. Valero, R. Costa, I. d. P. R. Moreira, D.G. Truhlar, F. Illas, Performance of the m06 family of exchange–correlation functionals for predicting magnetic coupling in organic and inorganic molecules, J. Chem. Phys. 128 (2008) 114103.

[79] H.S. Yu, X. He, S.L. Li, D.G. Truhlar, Mn15: A kohn–sham global-hybrid exchange–correlation density functional with broad accuracy for multi-reference and single-reference systems and noncovalent interactions, Chem. Sci. 7 (2016) 5032–5051, http://dx.doi.org/10.1039/C6SC00705H.

[80] P.Y. Ayala, H.B. Schlegel, Identification and treatment of internal rotation in normal mode vibrational analysis, J. Chem. Phys. 108 (6) (1998) 2314–2325, http://dx.doi.org/10.1063/1.475616, URL http://scitation.aip.org/content/aip/journal/jcp/108/6/10.1063/1.475616.

[81] R.L. Thorndike, Who belongs in the family? Psychometrika 18 (4) (1953) 267–276.

[82] C.R. Jacob, M. Reiher, Localizing normal modes in large molecules, J. Chem. Phys. 130 (8) (2009) 084106, http://dx.doi.org/10.1063/1.3077690.

[83] M. Mendolicchio, J. Bloino, V. Barone, Perturb-then-diagonalize vibrational engine exploiting curvilinear internal coordinates, J. Chem. Theory Comput. 18 (12) (2022) 7603–7619, http://dx.doi.org/10.1021/acs.jctc.2c00773, arXiv:https://doi.org/10.1021/acs.jctc.2c00773.

[84] V.P. Nicu, E.J. Baerends, On the origin dependence of the angle made by the electric and magnetic vibrational transition dipole moment vectors, Phys. Chem. Chem. Phys. 13 (2011) 16126–16129, http://dx.doi.org/10.1039/C1CP21442J.

[85] S. Góbi, G. Magyarfalvi, Reliability of computed signs and intensities for vibrational circular dichroism spectra, Phys. Chem. Chem. Phys. 13 (36) (2011) 16130–16133, http://dx.doi.org/10.1039/C1CP21645G.

[86] G. Longhi, M. Tommasini, S. Abbate, P.L. Polavarapu, The connection between robustness angles and dissymmetry factors in vibrational circular dichroism spectra, Chem. Phys. Lett. 639 (2015) 320–325, http://dx.doi.org/10.1016/j.cplett.2015.09.043, URL http://www.sciencedirect.com/science/article/pii/S0009261415007320.